Wheat crop biophysical parameters retrieval using hybrid-polarized RISAT-1 SAR data

Sugandh Chauhan[a], Hari Shanker Srivastava[b,*], Parul Patel[c]

[a] Department of Natural Resources, Faculty of Geo-Information Science and Earth Observation (ITC), University of Twente, Enschede, Netherlands
[b] Agriculture and Soils Department, Indian Institute of Remote Sensing (IIRS), Indian Space Research Organisation (ISRO), Dehradun 248001, India
[c] Space Applications Centre (SAC), ISRO, Ahmedabad 380015, India

ABSTRACT

The main goal of this study was to assess the potential of SAR backscatter signatures (RH and RV) retrieved from hybrid-polarized RISAT-1 SAR data in providing relevant information about the wheat growth parameters (leaf area index or LAI, plant water content or PWC, plant volume or PV and wet biomass or WB) over the entire growing season. The study was carried out over the parts of Bharatpur and Mathura districts located in Rajasthan and Uttar Pradesh (India), respectively. The three-date time series hybrid-polarized dataset was collected co-incident to which a comprehensive ground truth campaign was organised. We propose that refining the total backscatter (σ_{total}^{0}) values after minimising the effect of underlying/background soil cover, would result in more accurate retrieval of plant parameters since it is the vegetation backscatter, which ultimately has a direct cor-relation with the crop biophysical parameters. It was achieved using a semi-empirical water cloud model (WCM) based approach. The applicability of four different combinations of canopy descriptors, i.e. leaf area index (LAI), plant water content (PWC), leaf water area index (LWAI) and interaction factor (IF that takes into consideration the moisture distribution per unit volume) was tested on the RH and RV backscatter. We found that WCM based on LAI and IF as the two canopy descriptors modelled the total backscatter with a significantly high coefficient of determination (R^2 = 0.90 and 0.85, respectively) and RMSE of 1.18 and 1.25 dB, respectively. Subsequently, this set was used to retrieve the soil-corrected vegetation backscatter (σ_{veg}^{0}) values. A comparative evaluation of the retrieval accuracy between plant parameters estimated from σ_{total}^{0} ($\sigma_{T\_RH}^{o}$, $\sigma_{T\_RV}^{o}$) and σ_{veg}^{0} ($\sigma_{V\_RH}^{o}$, $\sigma_{V\_RV}^{o}$) was performed using rigorously trained multi-layer perceptron (MLP) neural networks. The findings suggest that the prediction accuracy considerably improved when the backscatter of underlying/background soil cover was eliminated. The designed networks (with σ_{total}^{0} as input) retrieved plant water content and plant volume with the highest accuracy of 0.82 and 0.80, respectively while it increased dramatically to 0.87 and 0.89 when the inputs were substituted by σ_{veg}^{0}. The present study is a first step towards retrieving crop parameters from hybrid-polarized data and thus possesses the potential to serve as a reference for further research initiatives.

1. Introduction

Accurate retrieval of the crop biophysical parameters is of crucial importance as they define the status of a crop at a particular time and are essential inputs to the crop yield models (Moulin et al., 1998; Doraiswamy et al., 2005; Patel et al., 2006b; Kogan et al., 2013). An accurate mapping and quantification of these parameters can be done on an extensive scale using remote sensing due to a high correlation between the observations derived from satellites and biophysical parameters (Ceccato et al., 2001; Colombo et al., 2003; Patel and Srivastava, 2013b; Battude et al., 2016). The availability of synthetic aperture (SAR) data, specifically at various polarizations, frequencies and incidence angles have started an era with enormous possibilities which have been exploited for various agricultural applications (McNairn et al., 2014; El Hajj et al., 2016). Due to its unique sensitivity towards crop moisture content, soil moisture, crop biomass, crop height, plant density etc., SAR can play a significant role in studies related to the monitoring of crop growth, soil moisture, crop dis-crimination, crop phenology and crop biophysical parameter retrieval (Patel et al., 2006a; Patel and Srivastava, 2007; Srivastava et al., 2006a, 2006b; Srivastava et al., 2009). However, due to its sensitivity to var-ious target parameters, retrieval of a desired target parameter is always a challenging task. For example, if a user is interested in soil moisture; crop cover, surface roughness and soil texture act as noise parameters,

whereas in case of crop biophysical parameter retrieval, the underlying/background soil moisture can interfere with the retrieval process.

Attempts have been made by many researchers to incorporate the effect of these noise parameters in soil moisture retrieval (Srivastava et al., 2002, 2003; Srivastava et al., 2006b). There is a substantial heritage of studies that have documented the usability and sensitivity of coherent dual (HH + VV or HH + HV or VV + VH)/quad-polarized (HH, HV, VH, VV) data to wheat crop characteristics either through ground-based experiments (Ulaby and Bush, 1976; Bouman, 1991), or by the means of airborne and space-borne SAR campaigns (Ferrazzoli et al., 1997; Saich and Borgeaud, 2000; Macelloni et al., 2001). However, the study reports that reduced swath width with increased pulse repetition frequency (PRF) (by a factor of 2) and data rate (by a factor of 4) in quad-pol satellite systems result in power and hardware complexities (Raney, 2007), making them less appropriate for large-scale routine coverage.

The compact polarimetry concept, first suggested in 1970 (Green, 1968) has been revived (Souyris et al., 2005; Raney, 2007) and is now at the frontier of current research. Hybrid polarimetry, a particular case of compact polarimetry, transmits circular (right/left) and receives dual linear (horizontal & vertical) polarized waves (RH, RV or LH, LV). In comparison to other dual/quad-pol systems, it can lead systems with less radio-frequency (RF) hardware and reduced mass (Raney, 2011). Souyris et al. (2005) showed that compact SAR is capable of providing similar information as that of fully polarimetric SAR for targets exhibiting azimuthally symmetric scattering. Raney (2007) also promoted the use of hybrid SAR owing to its simpler architecture and increased swath coverage in contrast to the traditional circularly polarized SAR (Green, 1968) and other polarimetric modes. Patel and Srivastava (2013b) carried out a comparative analysis and concluded that hybrid polarimetric mode with circular transmit linear receive is superior to quad-pol SAR backscatter alone for vegetation parameter retrieval. On the other hand, a probabilistic approach to soil moisture retrieval using RISAT-1 SAR data was found to be useful for improved soil moisture estimation for bare soil conditions as well as moderately vegetated terrain (Pal et al., 2017).

So far, the use of hybrid polarimetry has been realised only through the synthetic simulation of hybrid-polarized data from the quad-pol data (Charbonneau et al., 2010; Patel and Srivastava, 2013b). Indeed, the launch of ISRO's first indigenous space-borne hybrid-polarimetric SAR sensor onboard RISAT-1, operating in several spatial resolution/polarimetric modes has paved the way for researchers to exploit entirely new dimension of radar polarimetry (Misra et al., 2005). Calibration of the RISAT-1 SAR data is also a challenging task as it is first of its kind. Mishra et al. (2014) detail the outcome of the RISAT-1 SAR hybrid polarized FRS beam mode SAR data calibration using point target response. Very few studies have made use of RISAT-1 hybrid polarized SAR data to explore crop characteristics. Among the few, Uppala et al. (2016) successfully delineated a maize crop using a single date hybrid dual-polarimetric RISAT-1 SAR data with a spatial agreement of 91%. Sivasankar et al. (2015) analysed the sensitivity of different hybrid polarimetric parameters from RISAT-1 data for various land cover targets and found that the depolarization effect was very sensitive to the vegetation. Overall, the major focus of such studies has been on limited application areas like feature identification and classification accuracy assessment (Kumar et al., 2016). While few attempts have been made for wheat crop parameter retrieval using simulated hybrid-polarized SAR data (Patel and Srivastava, 2013b), an understanding of the sensitivity of hybrid-polarized data to the crop parameters, especially in the context of wheat has not been developed yet using RISAT-1 SAR; the first earth observing SAR that is providing hybrid polarized data. Thus, the primary objective of this investigation was to retrieve leaf area index (LAI), plant volume (PV), plant water content (PWC) and wet biomass (WB) of the wheat crop using hybrid-polarized RISAT-1 SAR data.

Over the past few years, studies by Taconet et al. (1994), Brown et al. (2003), Cookmartin et al. (2000) and Mattia et al. (2003) have illustrated the temporal variation of backscatter from the wheat crop, particularly at C-band. In particular, these studies have argued that the contribution of underlying/background soil surface attenuated by the canopy above dominate the backscatter response from such narrow leaf crops with a vertical structure, predominantly in the early growth stages. It is particularly the case in the range of incidence angles 20° to 40°. Even in the subsequent stages, the effect of soil cover cannot be entirely ignored. Thus, in the present study, an approach has been demonstrated to refine the total backscatter coefficient (σ_{total}^0) by eliminating the contribution from underlying/background soil cover (σ_{soil}^0).

In parallel, several modelling approaches have facilitated the understanding of interactions of the radar signal with vegetation and underlying/background soil cover. These models have evolved from simple process based Water Cloud Model or WCM proposed by Attema and Ulaby (1978) to more sophisticated Michigan Microwave Canopy Scattering or MIMICS model proposed by Ulaby et al. (1990) and have been validated on various crops like wheat, corn, rice, etc. using multiparametric SAR data (Toure et al., 1994; Dabrowska-Zielinska et al., 2007). At the same time, radiative transfer and analytic wave models with different approximations have also been used (Tsang et al., 1995; Del Frate et al., 2004). Although these physically based models may be theoretically sound in interpreting the measured data, the retrieval of crop biophysical variables with their inversion is still difficult due to the inherent complexity and intensive input requirements (Wang et al., 2009). To circumvent these limitations, a simpler semi-empirical WCM approach has been used in this study to model and refine σ_{total}^0.

The intensity of the received σ_{total}^0 is primarily dependent on the strength of coupling that takes place between the signal and the scatterers. This, in turn, is related to the sensor parameters (frequency, incidence angle or polarization) as well as the target characteristics (structure, dimension, orientation or dielectric properties). For instance, Macelloni et al. (2001) showed that the contribution from "broad-leaf" crops (corn or sorghum) could be conveniently modelled using the L-band data while lower wavelength (C-band) is more suitable for studying "narrow-leaf" crops (wheat or alfalfa). In C-band, the crop canopy behaves as an inhomogeneous medium with different plant constituents responding differently to the incident energy (Patel et al., 2006a). To facilitate the understanding of such complex interaction mechanisms, a robust model with adequate parameterisation needs to be generated (Ulaby et al., 1986). The assumptions made in WCM simplify the scattering processes in accordance with some physical canopy parameters/descriptors. However, the key element of consideration here is to differentiate and to correlate the most important crop parameters that would satisfactorily describe a crop canopy. Several WCM parametrization procedures have been tested to date (Prevot et al., 1993; Dabrowska-Zielinska et al., 2007; Said et al., 2012), however, none of them account for the structural inhomogeneity of a crop canopy solely in terms of a canopy descriptor. To this end, a potential combination of canopy descriptors have been suggested in this study and their effect on the σ_{total}^0 simulation have been evaluated.

The dependence of the σ_{total}^0 on multiple soil and vegetation parameters makes the inversion process quite cumbersome. Modelling of such non-linear processes based on simple relationships between σ_{total}^0 and crop biophysical parameters tends to be unreliable (Del Frate et al., 2004). A more advanced approach based on neural networks has shown promising results in modelling such non-linear processes and has been found to be particularly relevant for inversion with multi-dimensional inputs and outputs (Wang and Dong, 1997; Del Frate and Wang, 2001; Jia et al., 2013). Therefore, in this study, neural networks were adopted for the retrieval of wheat biophysical parameters. The networks were trained and validated using ground measurements, following which a comparative evaluation of the retrieval accuracy of crop parameters was done for the total as well as refined backscatter coefficients. Inevitably, the procedure does have some limitations, which have been critically examined in the paper. Nonetheless, it has the capability of
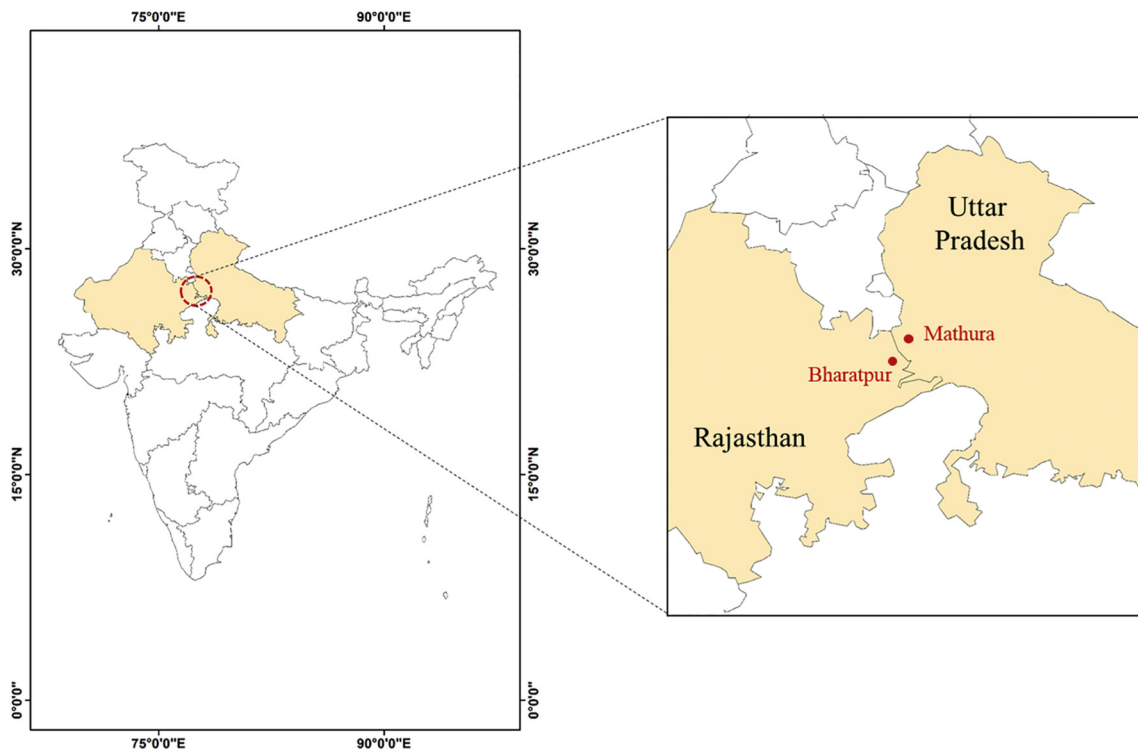
Fig. 1. Location map of the study site.

fully utilising the potential of the multi-temporal datasets for wheat biophysical parameter retrieval.

2. Materials and methods

2.1. Study site

The study was carried out over the parts of Bharatpur and Mathura districts located in Rajasthan and Uttar Pradesh (India), respectively (Fig. 1). The land is relatively flat, and wheat crop management practices are consistent throughout the area. Wheat is cultivated once a year during the December–April season. At the time of data acquisition, the weather conditions over the study area were quite stable. Wheat and mustard constituted the major crops while other minor crops like chickpea and potato were also planted in a few fields. The official time for full tillering (early-vegetative), booting/heading (late-vegetative) and milking/grain filling (mid-maturing) stages in the study site is late-January, mid-February and mid-March, respectively (Fig. 2). The majority of wheat fields in the region were greater than 600 m² in the area, but the row direction was not identical. Apart from this, there were abundant bare fields too (Fig. 3), making the site feasible to attain the specified objectives. A total of 220 (140 crop and 80 soil) samples were collected from wheat and bare fields over the period of January–March.

January is the coldest month of the year with average temperature of 15.7°. The precipitation is minimum in December at an average of 4 mm.

2.2. Experimental datasets

2.2.1. Remote sensing data

We used hybrid-polarized RISAT-1 SAR (SLC) images for the month of January, February and March 2015 in fine resolution stripmap (FRS-1) mode, spanning the crucial growth stages of wheat crop (Table 1). Indeed, the quantification of the parameters at these stages is of utmost importance for crop growth diagnosis and yield assessment studies. Three-date time-series data in the required hybrid polarized mode, at RH and RV polarizations was acquired with the revisit interval of 24 days and swath of 25 km. The images were acquired at a spatial resolution of 3 × 3 m on the ground. Selection of optimum SAR sensor parameters is essential for studies that aim at target parameter retrieval using SAR. Srivastava et al. (2008) have demonstrated that high incidence angle, SAR is more suitable for studies related to crop due to its longer path length and higher slant height inside the vegetation canopy. Accordingly, we chose an incidence angle of ~38°.

Fig. 2. Illustration of wheat canopies at (a) early-vegetative, (b) late-vegetative, and (c) mid-maturing stages, respectively.

Fig. 3. Bare fields during wheat crop growing season.

Table 1

RISAT-1 data acquisition date, sensor characteristics and the wheat growth stage captured.

RISAT-1 data acquisition date	Wheat growth stage	Sensor characteristics			
		Scene centre lat/long	Pass	Incidence angle	Time of acquisition
27 January 2015	Full tillering	27.168/ 77.457	Ascending	38.90274°	12:50:39.872
21 February 2015	Booting/ heading	27.139/ 77.407	Ascending	38.16588°	12:50:20.714
18 March 2015	Milking/ grain filling	27.185/ 77.408	Ascending	38.18430°	12:50:19.648

2.2.2. Design of experimental setup and field data collection

A statistical approach was utilised to obtain the minimum number of pixels (m) that need to be averaged from the SAR image and minimum size of the sampling unit (in m^2) that should be considered while doing the ground measurements. This approach takes the phenomenon of fading into account, due to which the random fluctuations in the return signal, coming from a specific scene location produces speckle on the image. By considering the error of 10% on the signal amplitude with 95% confidence interval, the value of m was estimated to be 105 while the minimum field size of 630 m^2 was considered for the ground measurements. Further details of this approach can be found in Patel and Srivastava (2013a).

We made detailed field observations of the crop and soil parameters simultaneous to the RISAT-1 satellite pass. We recorded the structural parameters like plant height, plant volume, wet biomass, plant density (per m^2), and LAI for each field. Additionally, we also noted down the

morphological variables such as leaf size, stem diameter and other observations related to the field condition, crop variety, growth stage, and soil moisture status. Nearly homogenous fields were selected. Within each field, we collected five crop and soil samples. We then averaged the measured values for the five points and considered the average value as representative for that field. The soil and crop samples were weighed to get fresh soil weights (sw_f) and wet biomass (cw_f). The corresponding surface roughness was also measured.

The LAI was measured with an AccuPAR LP-80 PAR/LAI Ceptometer while a GPS based mobile mapping unit was used to trace the field vector boundaries. A core sampler method was employed to get the bulk density of the soil samples (up to 5 cm). The crop and soil samples were dried (at Central Analytical Laboratory, Indian Institute of Remote Sensing) at 70 °C and 105 °C, respectively for 24 h in an electrically fitted oven with the digital temperature controller (Fig. 4b, d). The dried crop (dry biomass or cw_d) and soil (sw_d) samples were weighed again to get the volumetric soil moisture (M_v) and plant water content (PWC) using the following equations:

$$M_{gravi} \ (\%) = \left(\frac{sw_f - sw_d}{sw_d} \right) * 100 \tag{1}$$

$$M_v \ (\%) = M_{gravi} \ (\%) * \text{Bulk Density} \tag{2}$$

$$PWC \ (\text{kg/m}^2) = (cw_f - cw_d) \tag{3}$$

where M_{gravi} is the gravimetric soil moisture.

Additionally, we immersed the plant samples into the water-filled graduated measuring cylinders and measured the amount of water displaced to compute the volume of each plant component (Fig. 4a). The field measurements and the subsequent laboratory analysis, therefore, resulted in two categories of collected variables: the non-destructive variables such as the plant density (plants/m^2), LAI (m^2/ m^2), plant height (m) and the destructive variables such as wet biomass
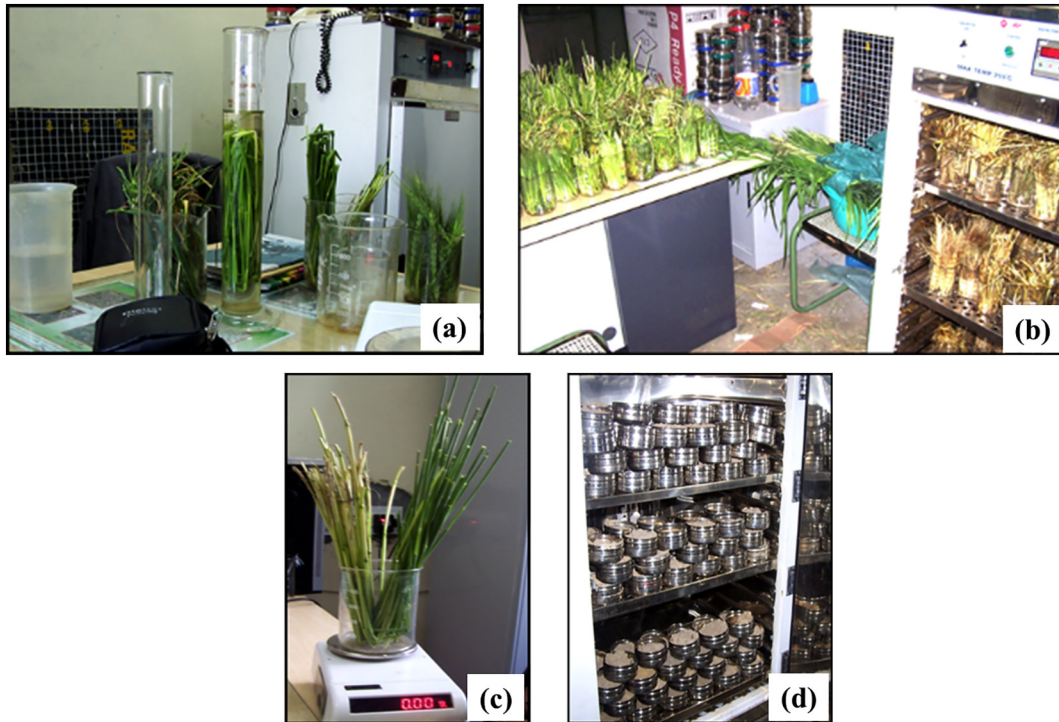
Fig. 4. Laboratory analysis of (a) plant volume, (b) dry biomass, (c) fresh biomass and (d) soil moisture.

(kg/m^2), dry biomass (kg/m^2), plant water content (kg/m^2), plant volume (cm^3/m^2) and volumetric soil moisture (%).

Fig. 5 depicts the overall methodological flowchart adopted in this study. The main steps comprise of (a) model development, and (b) retrieval and validation. The primary inputs and outputs (illustrated as parallelograms) have been colour-coded as yellow and green,

respectively.

2.3. Pre-processing of RISAT-1 Synthetic Aperture Radar images

The acquired SAR data was radiometrically calibrated into the σ^o images (RH and RV) using Eq. (4). The RH and RV backscatter images
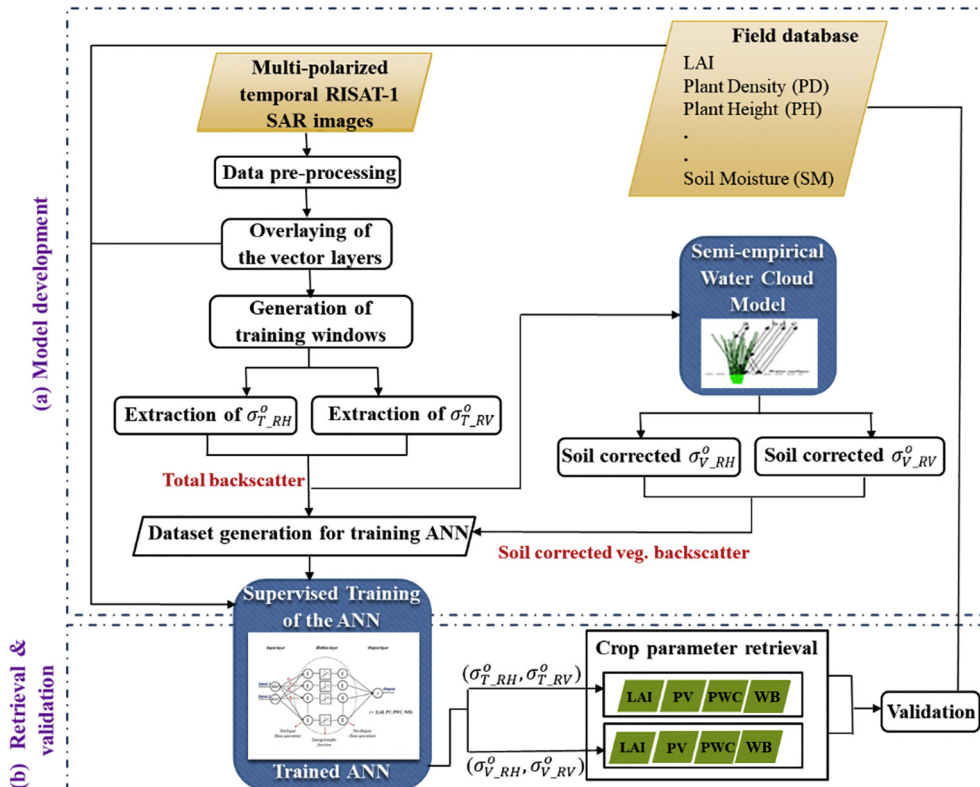

Fig. 5. The methodology adopted for wheat biophysical parameters retrieval using water cloud model (WCM) and neural networks (NN).

RV Backscatter Image

RV_Jan 27   RV_Feb 21   RV_Mar 18

(a)

RH Backscatter Image
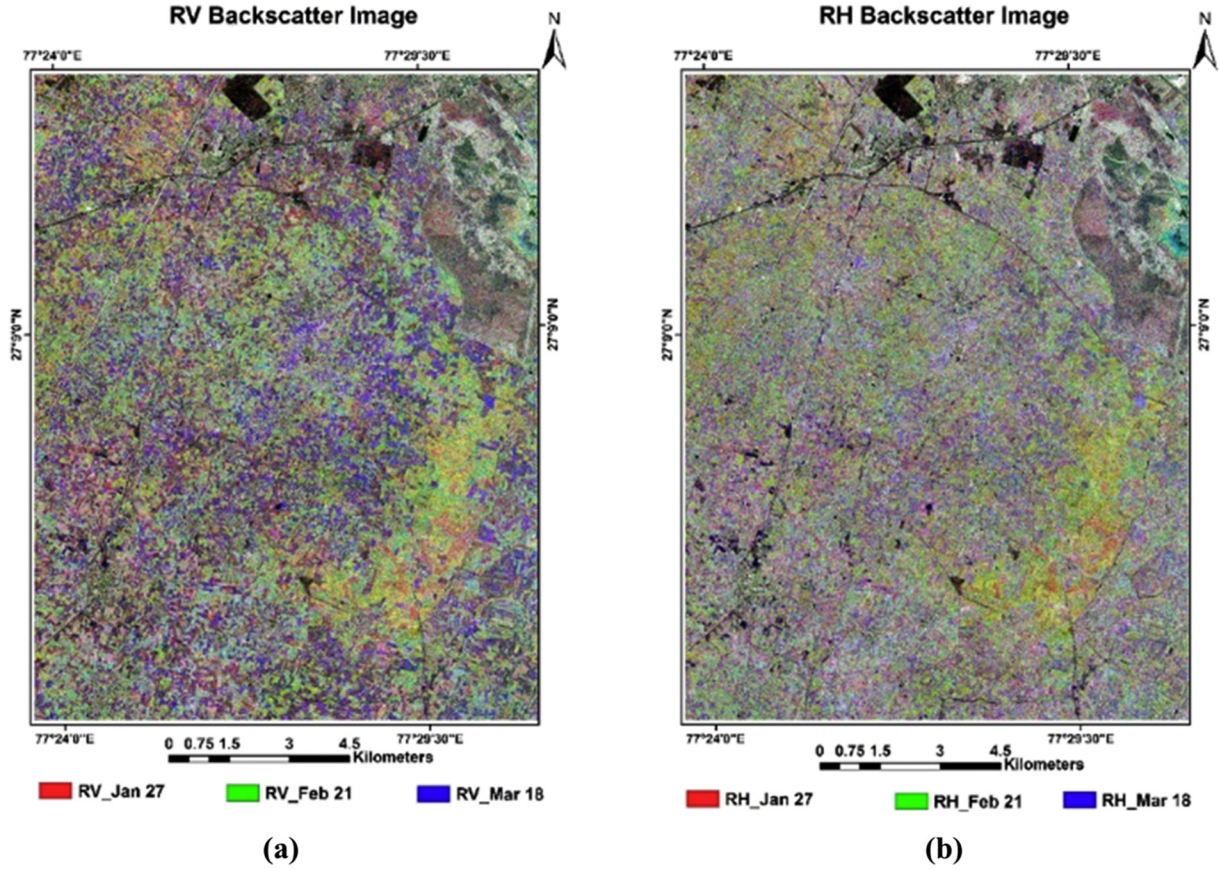

RH_Jan 27   RH_Feb 21   RH_Mar 18

(b)

Fig. 6. (a) RV and (b) RH backscatter images.

have been illustrated in Fig. 6.

$$\sigma_p^0 \text{ (dB)} = 20\log_{10}(DN_p) - K_{cal\,sigma0,dB} + 10\log_{10}(\sin(i_p)/\sin(i_{center})) \quad (4)$$

where, σ_p^0 (dB) is the radar backscatter coefficient (Sigma0) in dB for the pixel p; DN_p is the digital number for the pixel p; $K_{cal\,sigma0,\,dB}$ is the product calibration constant in dB; i_p is the incidence angle for the pixel p, and i_{center} is the incidence angle at the scene centre.

The temporal σ^o images were then geo-referenced & co-registered using high-resolution satellite imagery of same resolution (3 m). A second order polynomial transformation with the nearest neighbourhood sampling approach was applied. Furthermore, to suppress the speckle noise and preserve the edge information, an enhanced Lee filter with the moving window of 3 × 3 was applied to the images using ENVI 5.0 software. After the necessary preprocessing, GPS vector layers of the field boundaries traced during the field observations were overlaid on the co-registered set of images and the signatures were extracted, both for wheat fields as well as the bare field locations. As a measure of precaution, we compared the extracted mean σ^o values from the filtered image to those derived from the raw data, and we found that their differences were negligible (< 0.05 dB).

2.4. Parameterisation of water cloud backscatter model

The water cloud model (WCM) developed by Attema and Ulaby (1978) is a first-order approximation of the radiation transfer taking place throughout the vegetation canopy and relies on the assumption that a canopy can be modelled as a collection of uniformly distributed water droplets held structurally in place by its dry matter. The general expression for the total power backscattered (σ_{total}^o) by the crop canopy is given by following equations.

$$\sigma_{total}^o \text{ (dB)} = \sigma_{veg}^o + L^2 \cdot \sigma_{soil}^o \quad (5)$$

with, σ_{veg}^o (dB) $= A \cdot V_1 \cdot \cos\theta(1 - L^2) \quad (6)$

$$L^2 = \exp(-2B \cdot V_2 \cdot \sec\theta) \quad (7)$$

$$\sigma_{soil}^o \text{ (dB)} = C + D \cdot M_v \quad (8)$$

where, σ_{veg}^o and σ_{soil}^o are the backscatter coefficients for vegetation and soil in dB, respectively; L^2 is the two-way attenuation factor (through the canopy); θ is the incidence angle, V_1 and V_2 are the canopy descriptors; A, B and C, D are the vegetation and soil specific coefficients, respectively (Prevot et al., 1993). For a given level of roughness, the σ_{soil}^o may be related to the volumetric soil moisture (M_v) by Eq. (8). This linear relationship between σ_{soil}^o and M_v is based on the experimental evidence, which suggests that for a given soil roughness and M_v, the σ_{soil}^o may not follow a linear trend, but for agricultural-based applications where the soil moisture range is between 5 and 40%, a linear trend can be fitted for broader area applications (Attema and Ulaby, 1978). The deviation between the values estimated by linear and non-linear approximations may be quite high if the M_v values are below 10% (Ulaby et al., 1986). However, in the present study site, since the minimum value of M_v was above this threshold, there was no scope of possible error propagation through the model.

The impact of soil roughness was undermined to develop an operational model and was thus taken as more or less constant during the multi-temporal observations. This assumption is based on the fact that it produces only a vertical shift in the σ_{soil}^o, without influencing the overall trend, thus making soil moisture variability a sole factor for the change in signal (Quesney et al., 2000; Hégarat-Mascle et al., 2002). Furthermore, even the estimated parameter B is unaffected by this offset value. On substituting Eqs. (6), (7) and (8) in Eq. (5), it gives:

$$\sigma_{total}^o \text{ (dB)} = \{A \cdot V_1 \cdot \cos\theta_i [1 - \exp(-2B \cdot V_2 \cdot \sec\theta_i)]\} + \exp(-2B \cdot V_2 \cdot \sec\theta_i)$$
$$\cdot (C + D \cdot M_v) \quad (9)$$

Table 2
Canopy descriptors tested in WCM.

	V_1	V_2
Scenario I	LAI	LAI
Scenario II	LAI	PWC
Scenario III	LWAI	LWAI
Scenario IV	LAI	IF

The variation in the canopy descriptors is mainly due to the complexity of the canopy structure and relative simplicity of the model being used to account for the total canopy backscatter (Dabrowska-Zielinska et al., 2007). Due to the dependence of $\sigma_{total}{}^o$ on geometrical and dielectric plant properties along with the unavailability of any predefined theoretical basis for the selection of the best set of descriptors, a set of cases (Table 2) were framed to testify their performance in modelling the $\sigma_{total}{}^o$.

The LAI or leaf area index (m²/m²) is one of the most well-known and widely used descriptors. PWC or Plant Water Content (kg/m²) is the amount of water present in the crop sample and was obtained using Eq. (3). The LWAI or leaf water area index (unitless) (Dabrowska-Zielinska et al., 2007) refers to the quantity of water extended in the leaf area and is defined as:

$$LWAI = LAI \cdot W \tag{10}$$

with,

$$W = \frac{cw_f - cw_d}{cw_d} \tag{11}$$

Apart from these, the IF or interaction factor (conceptualised by Patel et al., 2006a) was tested as a potential descriptor to account for the vertical inhomogeneity of the crop canopy. In a crop field, the SAR backscatter is influenced by the density, moisture content, plant structure and volume of each of the plant components (namely head, stem and leaf), in addition to the soil moisture (Ulaby and Wilson, 1985; Bouman and van Kasteren, 1990). The distribution of moisture and volume varies heterogeneously along each component, and this determines the depth of penetration of SAR signal into the crop (which in turn affects the resultant backscatter). Patel et al. (2006a) experimentally incorporated these factors into a unique plant parameter called interaction factor (IF), the formulation of which is as follows:

$$IF_{whole\ plant} = \frac{(Plant\ moisture * Volume\ of\ plant * Plant\ density)}{Plant\ height}$$

$$= \frac{(PWC * V_p * N)}{h} \tag{12}$$

We tested these four approaches for evaluating the performance of WCM. The coefficients C and D were estimated by regressing the in situ M_v measurements with the RH and RV backscatter coefficients separately while for the estimation of A and B coefficients, iterative parameterisation was applied by minimising the following objective function:

$$SSE = \sum_{i=1}^{n} (\sigma_{i,obs}^{o} - \sigma_{i,est}^{o})^2 \tag{13}$$

Here, SSE is the sum of squared errors; n refers to the total number of observations; $\sigma_{i,\ obs}{}^o$ and $\sigma_{i,\ est}{}^o$ refers to the observed (from SAR image) and estimated (from WCM) backscatter coefficients for each observation i. The WCM Eq. (9) was passed as a fitness function f to the Matlab nonlinear least-squares solver *lsqnonlin* while the algorithm was set to Levenberg-Marquardt (LM). LM algorithm combines the advantages of steepest descent and Gauss-Newton method and has been recommended for optimizing multivariate non-linear problems due to its operating stability and accelerated convergence (Marquardt, 1963; Lourakis, 2005). The parameterisation that modelled the $\sigma_{total}{}^o$ with highest overall accuracy was used to refine the backscatter values by eliminating the contribution of underlying/background soil ($\sigma_{soil}{}^o$). It is proposed that the soil corrected vegetation backscatter coefficient ($\sigma_{veg}{}^o$) has a better correlation with the crop biophysical parameters than the total backscatter ($\sigma_{total}{}^o$).

2.5. Training and configuring neural networks

A neural network (NN) is a complex adaptive system that is composed of simple processing units called neurons, which work in parallel and try to learn the underlying patterns between the input-output pairs by constantly adjusting the synaptic weights. The inputs are fed into a hidden layer (where the real transformation and computation takes place), which may even be fed into layers of more hidden neurons and then eventually to the output layer. Each node in the hidden layer possesses a transfer function, which acts upon the net input it receives and estimates the layer's output, making it suitable to address non-linear problems, whose analytical solution might not be available (Jia et al., 2013).
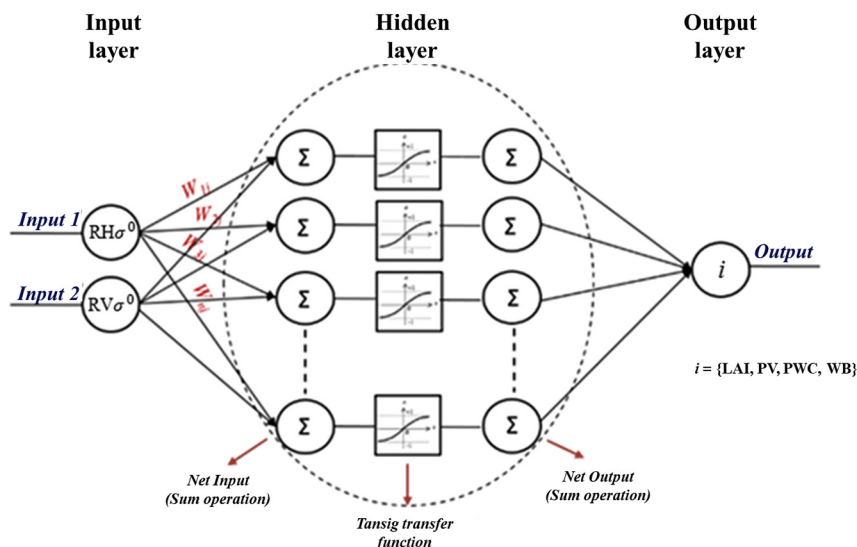

Fig. 7. The NN structure configured in the study.

Table 3
Training algorithms, neural network (NN) topology and RMSE threshold defined for different neural network architectures.

| Crop parameters	σ_{total}^{0} ($\sigma_{T\_RH}^{o}$, $\sigma_{T\_RV}^{o}$)		σ_{veg}^{0} ($\sigma_{V\_RH}^{o}$, $\sigma_{V\_RV}^{o}$)		RMSE threshold
	Training algorithm	NN topology	Training algorithm	NN topology	
LAI	Resilient backpropagation (RB)	$2 \times 23 \times 1$	Levenberg-Marquardt (LM)	$2 \times 18 \times 1$	$1\,m^2/m^2$
PV	Levenberg-Marquardt (LM)	$2 \times 20 \times 1$	Levenberg-Marquardt (LM)	$2 \times 22 \times 1$	$1.50\,cm^3/m^2$
PWC	Levenberg-Marquardt (LM)	$2 \times 23 \times 1$	Bayesian regularization (BR)	$2 \times 18 \times 1$	$0.5\,kg/m^2$
WB	Levenberg-Marquardt (LM)	$2 \times 24 \times 1$	Bayesian regularization (BR)	$2 \times 18 \times 1$	$0.5\,kg/m^2$
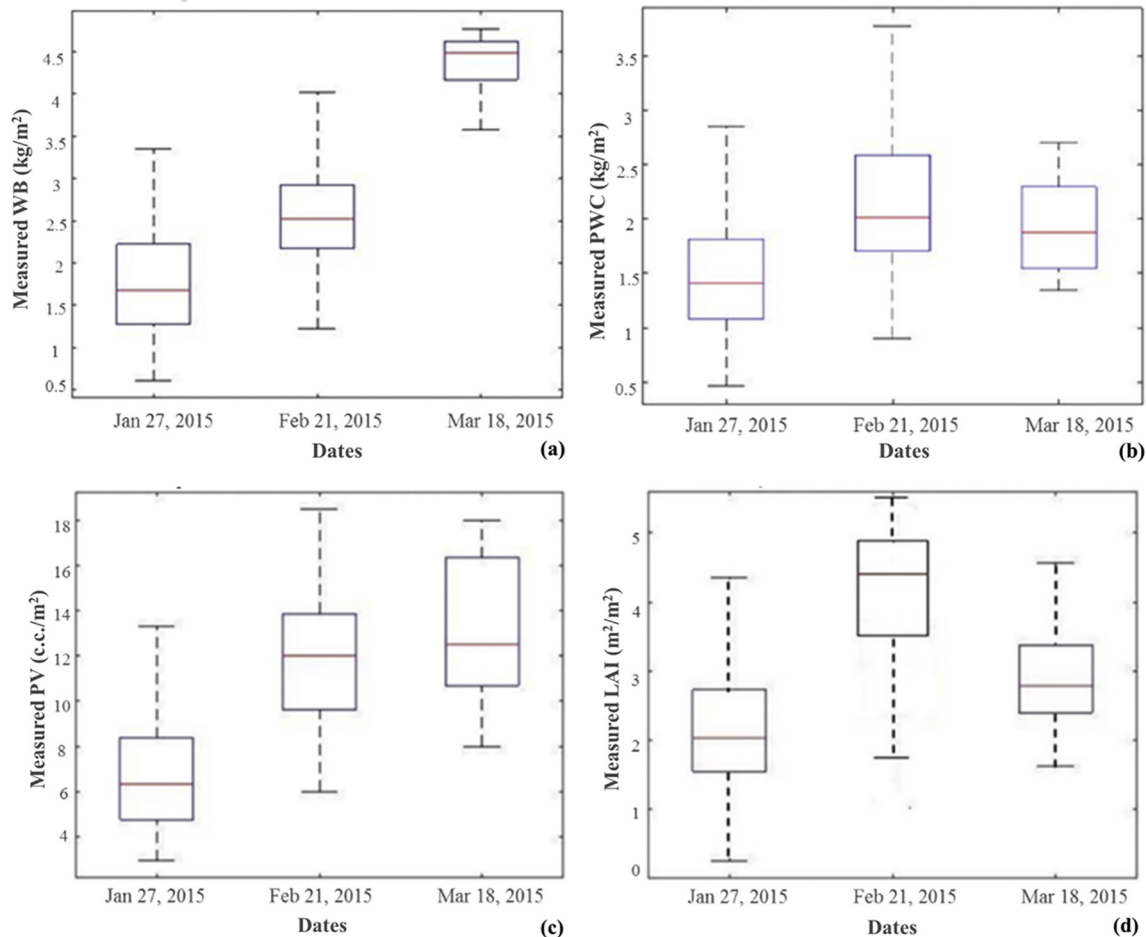
Fig. 8. Temporal variation of the plant variables; (a) wet biomass, (b) plant water content, (c) plant volume, and (d) LAI, over the growing season (number of samples $N = 140$).

We configured a total of eight standard multi-layer perceptron (MLP) NN architectures (Fig. 7) to retrieve four biophysical parameters of wheat crop, i.e. leaf area index (LAI), plant volume (PV), plant water content (PWC) and wet biomass (WB), from the total ($\sigma_{T\_RH}^{o}$, $\sigma_{T\_RV}^{o}$) as well as vegetation ($\sigma_{V\_RH}^{o}$, $\sigma_{V\_RV}^{o}$) backscatter coefficients, respectively. Following the basic preprocessing of the data points, we rigorously trained the networks in batch mode. To do so, detailed ground measurements constituted the training subset (90%), whereby n sets of backscatter coefficients [($\sigma_{T\_RHi}^{o}$, $\sigma_{T\_RVi}^{o}$) or ($\sigma_{V\_RHi}^{o}$, $\sigma_{V\_RVi}^{o}$) with (i = 1, 2, 3…n)] were fed as input while the corresponding n crop parameters [W_{LAIi} or W_{PVi} or W_{PWCi} or W_{WBi}] were supplied as desired output values. We again sub-divided the training subset into 80%-10%-10% ratio, respectively for training, testing and validation process. Thus, each network comprised of two nodes in the input layer while one node depicted the output layer. Table 3 shows the algorithms, topology and the RMSE threshold that was set for each architecture.

Additionally, we evaluated the performance graphs in each case to

see if any overfitting had occurred. We also analysed the test and validation curves to check if the test curve had witnessed a substantial increase before the validation curve did. If this was the case, then it meant that some overfitting might have occurred and therefore, the training process had to be repeated.

We determined the number of hidden layers/nodes and the training algorithm to be utilised by a trial and error method (Table 3). A single hidden layer in all the architectures provided reasonable results with the manageable computational load. Since the network may not be able to extrapolate beyond the input range that is supplied to it while training, we made sure that the training dataset spanned across the entire input range for which the network ultimately had to be used, so that the network could generalize well. Moreover, the entire dataset was iteratively randomised (~5–6 times) while repeatedly training the network for each set so that any inherent dependency of the retrieved results on the sampling procedure could be circumvented. We assessed the validity of trained networks using an independent validation (10%)
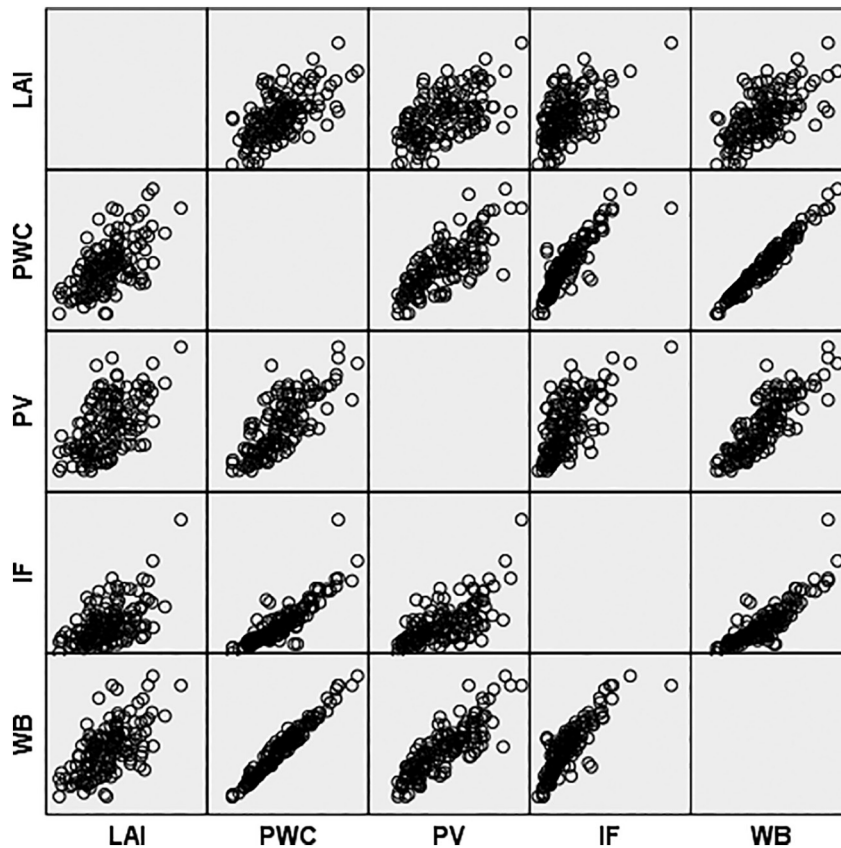
Fig. 9. Scatter plot showing a relative correlation between leaf area index (LAI), plant water content (PWC), plant volume (PV), interaction factor (IF) and wet biomass (WB).

set across the season. The NN was implemented in the Matlab software (http://www.mathworks.com/) by the combined use of the NN toolbox and manual scripting capabilities.

The performance of WCM and NN was evaluated using the conventional RMSE, Mean Absolute Percentage Error (MAPE) and Index of Agreement (IA) statistical measures. The formulation is as follows:

$$MAPE(\%) = \frac{\sum_{i=0}^{n} \left| \frac{a_i - p_i}{a_i} \right|}{n} * 100, \quad (a_t \neq 0) \tag{14}$$

$$IA = 1 - \frac{\sum_{i=0}^{n} (a_i - p_i)^2}{\sum_{i=0}^{n} ((|p_i - a_{mean}| + (|a_i - a_{mean}|))^2} \tag{15}$$

where a_i and p_i is the actual and predicted values, respectively while a_{mean} is the mean of the actual observations.

3. Results

3.1. Multi-temporal trends of crop biophysical parameters over the growing season

We collected the crop and soil samples from crop covered and bare fields coincident to the acquisition of satellite imageries on different dates. The availability of multi-temporal datasets enabled the monitoring of wheat crop cycle. Fig. 8 shows the box plots depicting the temporal variation of the critical crop parameters over the growing season.

We witnessed some key trends concerning the temporal behaviour of the crop variables collected over the fields. Since only a three-date dataset was available spanning across the tillering to milking/initial maturation stage of the wheat crop, subsequent interpretations regarding the crop variables would be made considering this point. As is

evident from Fig. 8a, the wet biomass values showed an overall increasing trend over the season. In January, the mean WB was as close to ~1.5 kg/m² but steadily moved upwards to the mean value of almost ~4.7 kg/m² as the crop progressed towards the milking/grain filling stage. It is primarily due to the modifications that the crop undergoes as it grows, considering the growth in the number of stalks and leaves. The flag leaves and ears start to appear at a later stage, and once the crop reaches its final maturity (by the end of March), it starts to dry up, causing the stem and leaf biomass to drop while the ear biomass may remain constant or increase slightly (Mattia et al., 2003). The plant volume showed an increasing trend in the initial months, i.e. till mid-February whereby it rose from the mean value of ~5.8 to 12 cm³/m², after which it got saturated. It could have been due to the combined effect of the increase in biomass and crop density per unit area.

The variation in the LAI values (Fig. 8d) depicted that LAI of wheat crop developed to almost 2 m²/m² from emergence to tillering stage, after which a fast growth was witnessed, causing the LAI values to surge to the maximum of ~4.7–6.1 m²/m² at the booting stage (in February). The emergence of first awns from the flag leaf sheath with the head enforcing the sheath to open markedly ended this stage. After that until the milking stage, the LAI values dipped to the mean value of 2.5 m²/m². Post-field analysis revealed that apart from different phenological stages, secondary environmental factors and agronomic treatments given to the fields had induced such broad range distribution of the LAI values. We observed a similar trend in case of plant water content (PWC). The PWC values first increased from 0.5–1.5 kg/m² in January end to almost 2–4 kg/m² during mid-Feb before finally dropping in the mid-March (Fig. 8b). The phenological stage of a crop extensively governs the plant water content, and thus its dielectric properties. Studies reveal that a good correlation exists between PWC and LAI (Ferrazzoli et al., 1992) causing a similar variation. The above trends in the crop variables are in close agreement with the studies carried out by
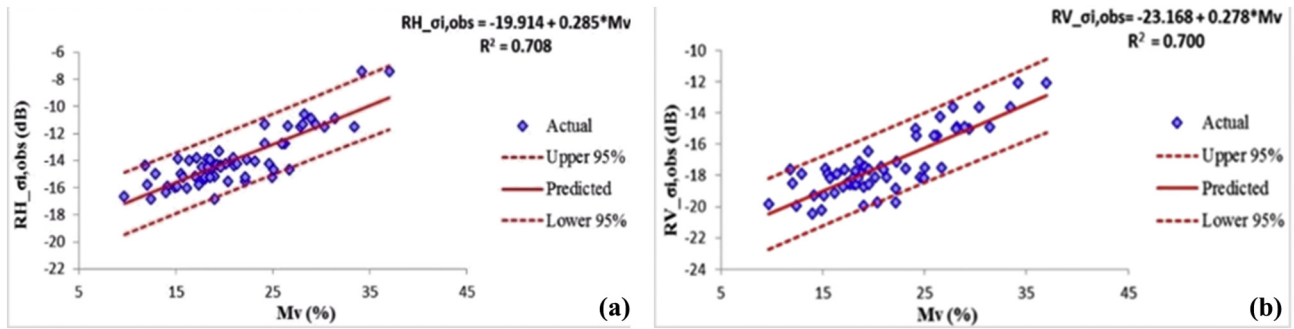
Fig. 10. The relationship between observed (a) σ^o_{RH}, (b) σ^o_{RV} and volumetric soil moisture (%) for bare field locations (number of samples $N = 80$).

researchers like Macelloni et al. (2001), Mattia et al. (2003), Del Frate et al. (2004) and Jia et al. (2013).

Since measured field variables such as LAI, PWC, PV, WB and LAI along with parameters like LWAI and IF derived from them are used heavily to calibrate the WCM and the neural network inversion model, the relationship of these parameters with each other is shown in Fig. 9.

3.2. Impact of different calibration methodologies on water cloud model performance

We regressed the in situ volumetric soil moisture measurements (M_v) with RH and RV backscatter coefficients separately to estimate the WCM soil parameters C and D. The gravimetric soil moisture values (M_{gravi}) in the area ranged from 6.9% to the maximum of 30% while the bulk density values ranged from 1.1 to 1.35 g/cm^3. Reasonably good coefficient of determination (R^2) was observed between RH ($R^2 = 0.71$), RV ($R^2 = 0.70$) backscatter coefficients (σ_{soil}^0) and volumetric soil moisture values (M_v) for all the fields (Fig. 10), which corroborated the fact that σ^o_{RH} and σ^o_{RV} are more or less equally sensitive to M_v.

The coefficients D and C in the model (Fig. 10, Eq. (8)) determine the effect of soil moisture and its roughness on the σ^o, respectively. The empirical relation was calibrated for the given soil type and the specific sensor configuration (C-band, incidence angle $\theta = 38.9$). The soil moisture sensitivity factor D was estimated as 0.285 and 0.278 for RH and RV, respectively, while the parameter C came out to be -19.914 and -23.168, respectively. A similar range of C (-11.93) and D (0.23) values have been reported by Srivastava et al. (2011), using RADAR-SAT-1 SAR data at HH polarization. Zribi and Dechambre (2003) also calculated the given parameters in a comparable range (-13.82 and 0.22, respectively) at 39° HH polarization. The estimated C and D coefficient values thus fall within a permissible range and are in line with the previous experiments. The difference can be attributed to different polarization used in this study.

Apart from this, determination of the best set of canopy descriptors (V_1 and V_2) is the most crucial step and decides the ultimate success with which the model is executed. Therefore, the next section will illustrate four different combinations of V_1 and V_2 that were tested in the model and the resulting accuracies with which they estimated σ_{total}^0. The most suitable combination along with the optimized coefficient values (A, B, C, D) was then used to determine σ_{veg}^0. Table 4 indicates the statistical indices used to evaluate the model performance for different scenarios. The number of observations used for model calibration and model validation has been depicted as $N_{obs,cal}$ and $N_{obs,val}$, while the degree of model fitting between observed and estimated σ_{total}^0 ($\sigma_{T\_RH}^o$, $\sigma_{T\_RV}^o$) values have been indicated with the coefficient of determination (R^2). Furthermore, RMSE, MAPE and IA measures have been used to validate the model prediction accuracy.

In the scenario I, LAI variable was used (as V_1 and V_2) to represent the effect of vegetation on the backscatter signal. Prevot et al. (1993) and Moran et al. (1998) implemented the WCM for crops like wheat,

Table 4
Model fitting parameters for different canopy descriptors.

Canopy descriptors		$N_{obs,\ cal}$	$N_{obs,\ val}$	R^2	RMSE (dB)	MAPE (%)	IA
V_1	V_2						
C 38.9°RH							
LAI	LAI	100	20	0.55	2.21	18.25	0.60
LAI	PWC	100	20	0.67	2.10	17.00	0.61
LWAI	LWAI	100	20	0.72	1.81	15.12	0.68
LAI	IF	100	20	0.90	1.18	9.61	0.80
C 38.9°RV							
LAI	LAI	100	20	0.40	3.53	19.12	0.55
LAI	PWC	100	20	0.69	2.02	10.75	0.74
LWAI	LWAI	100	20	0.72	1.93	10.01	0.79
LAI	IF	100	20	0.85	1.25	5.44	0.86

alfalfa, and cotton. In these works, the value of parameter A was set as 0 (for C-band), which is equivalent to considering the vegetation contribution as negligible. The parameter B that is known to characterise the attenuation of backscatter signal by the canopy was set as 0.089 and 0.09, respectively. However, in the context of this study, the non-zero value of parameter A (0.0378, 0.0254 for RH and RV, respectively) while a slightly lower value of parameter B (0.0255, 0.0147 for RH and RV, respectively) indicated that the contribution from the vegetation was quite significant and thus could not be neglected. The R^2 between observed and estimated RH backscatter values was 0.55 while for RV it was relatively on the lower side (Table 4). Unfortunately, the model did not perform well, since the RH and RV backscatter values were highly overestimated with high RMSE and MAPE values as is evident from Fig. 11a and b.

In scenario II, we used the crop variables LAI (V_1) and PWC (V_2) as a test case. In contrast to the previous model, incorporating these parameters together in the parameterisation of the backscatter resulted in a notable increase in the R^2 (0.67 and 0.69) between the observed and model-estimated σ^o_{RH} and σ^o_{RV} values, respectively (Table 4, Fig. 11c, d). Although the overall prediction accuracy increased, RMSE and MAPE values declined by merely 5% and 1.25% in the case of σ^o_{RH}. Relatively, the decline was quite significant in the case of σ^o_{RV} whereby the values markedly reduced by 42.7% and 8.3%, respectively while IA increased sharply by 34%.

In the third approach, we used LWAI as a potential canopy descriptor. Since this variable encompasses both leaf area and dielectric properties into one factor, we observed that it influenced the total σ^0 more effectively. As is evident from Table 4, the model performance marginally improved with the R^2 of 0.72 for both σ^o_{RH} and σ^o_{RV}. Similarly, the RMSE gradually lowered by 0.4 and 0.3 dB in contrast to the scenario I and II for σ^o_{RH}, while for σ^o_{RV}, it steeply dropped by 1.6 dB with respect to scenario I. On the contrary, the relative decline in RMSE with respect to scenario II was non-significant (0.09 dB). This is further illustrated in Fig. 11e and f. Even the study done by Dabrowska-Zielinska et al. (2007) have led to similar findings. We also tested the
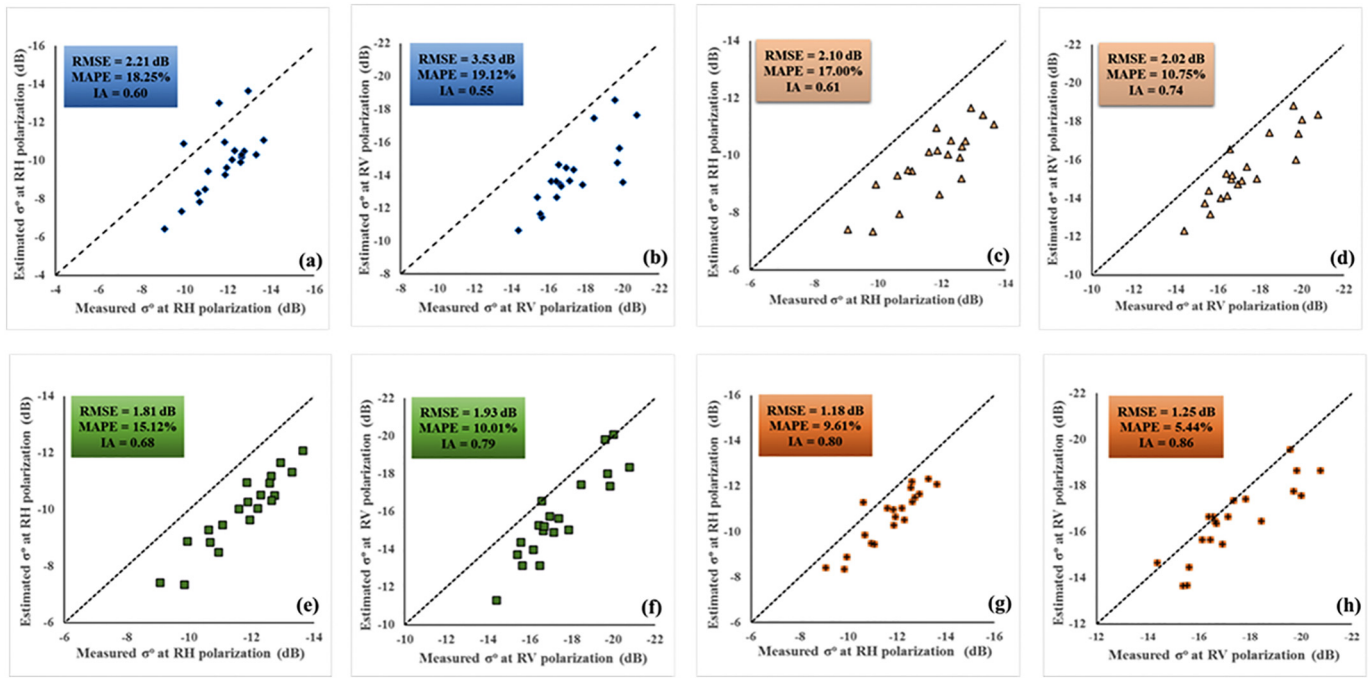
Fig. 11. Comparison of measured and WCM-estimated σ^o_{RH} (a, c, e, g) and σ^o_{RV}. (b, d, f, h) for (a), (b) V_1 = LAI, V_2 = LAI; (c), (d) V_1 = LAI, V_2 = PWC; (e), (f) V_1 = LWAI, V_2 = LWAI; and (g), (h) V_1 = LAI, V_2 = IF.

model performance with LAI and LWAI as a potential combination, but the improvement was non-significant. Thus, we did not discuss this model in further detail.

Finally, the applicability of LAI and IF as the canopy descriptors was tested. Table 4 reveals that with the use of LAI and IF, R^2 increased up to 0.90 with almost 46, 43.8 and 34.8% reduction in RMSE as compared to scenarios I, II and III, respectively for σ^0_{RH} while for σ^0_{RV}, the comparative decline was 64.5, 38 and 35.2% with highest R^2 of 0.85. The lowest MAPE and RMSE values testified that this model could be used further to retrieve the vegetation backscatter ($\sigma_{veg}{}^o$) values for the same fields. For illustration purposes, the model validation results have been presented in Fig. 11g and h for σ^o_{RH} and σ^o_{RV}. The model slightly overestimated the backscatter values, but the error in comparison to previously tested models was considerably lower.

3.3. Crop parameter retrieval accuracy from total and vegetation backscatter coefficients

A preliminary analysis of the relationships between field-measured crop parameters, and satellite/WCM derived measurements confirmed the sensitivity of the parameters to the C-band hybrid-polarized backscatter data. As discussed previously, we rigorously trained the neural networks to have a proper mapping between input (RH, RV) backscatter coefficients and crop biophysical parameters. The key to successful utilisation of neural network approach is to identify a comprehensive and explanatory set of input elements that, when taken compositely, give fine segregation in the mapping of the output variables. Thus, the

combined effect of multi-polarized RH and RV data has been tested.

Table 5 outlines the R^2 and error statistics (i.e. RMSE, MAPE, and IA indicators) for each parameter. Ideally, the RMSE values are expected to be close to zero, meaning that on an average, the model estimated values would be equal to the observed ones. But given the complexity of estimating these crop parameters based on SAR data, owing to high degree of non-linearity associated with the crop and satellite-derived parameters and also the inherent dynamicity of the variability that exists among the crop biophysical parameters over the growing season, it can be concluded that the above RMSE values are fairly close to zero. Since the SAR signal is known to interact with the crop at an oblique angle, the impact of incidence & azimuth angle relative to the field orientation may result in some secondary errors. Nonetheless, the flexibility provided by SAR sensors regarding the control that can be exercised on the sensor parameters compensates for this problem and may be worked upon to achieve higher accuracy.

3.3.1. Leaf area index (LAI)

While retrieving LAI by taking $\sigma_{total}{}^0$ ($\sigma_{T\_RH}{}^o, \sigma_{T\_RV}{}^o$) as input, the number of nodes in the hidden layer was kept as 23 since it was found that the network performance saturated beyond 23 nodes. Thus, the neural network with 2-23-1 (#neurons in input-hidden-output) configuration was selected for the LAI retrieval (Table 3). However, the overall R^2 of the selected network was quite low (R^2 = 0.70) (Table 5), even though the RMSE in training phase was as low as 0.72 m²/m². On validating the network performance with an independent dataset of 12 points taken across the season, the RMSE came out to be 0.77 m²/m²

Table 5
Parameter wise R^2 and error statistics (RMSE, MAPE, and IA) for $\sigma_{total}{}^0$ and $\sigma_{veg}{}^0$.

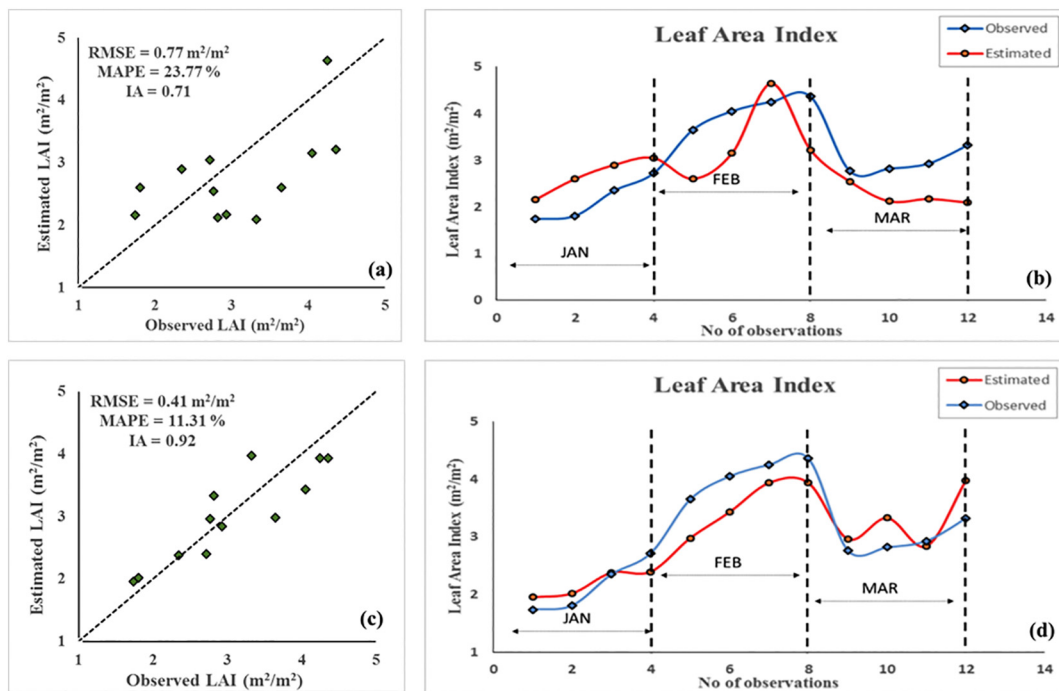| Crop parameters	$\sigma_{total}{}^0$ ($\sigma_{T\_RH}{}^o, \sigma_{T\_RV}{}^o$)				$\sigma_{veg}{}^0$ ($\sigma_{V\_RH}{}^o, \sigma_{V\_RV}{}^o$)			
	R^2	RMSE	MAPE (%)	IA	R^2	RMSE	MAPE (%)	IA
LAI	0.70	0.77 m²/m²	23.77	0.71	0.76	0.41 m²/m²	11.31	0.92
PV	0.80	1.51 cm³/m²	17.82	0.94	0.89	0.85 cm³/m²	10.31	0.98
PWC	0.82	0.38 kg/m²	22.60	0.81	0.87	0.17 kg/m²	10.00	0.95
WB	0.63	0.45 kg/m²	16.32	0.46	0.74	0.25 kg/m²	8.45	0.90

Fig. 12. Scatter plot (a, c) & multi-temporal (b, d) variation of the observed and estimated LAI across the season (number of samples $N = 12$). a, b correspond to the crop parameters retrieved from σ_{total}^0 ($\sigma_{T\_RH}^o, \sigma_{T\_RV}^o$) and c, d correspond to those retrieved from σ_{veg}^0 ($\sigma_{V\_RH}^o, \sigma_{V\_RV}^o$).

(Table 5) with quite a low IA (0.71). The comparable RMSE values of calibration and validation dataset shows that the model was able to train and generalize well, but only 70% of the variance in LAI could be explained by using σ_{total}^0 as the input. Fig. 12a and b shows a scatter plot and multi-temporal variation between the observed and estimated LAI at three different stages with σ_{total}^0 as input (Jan: full tillering; Feb: booting/heading; Mar: milking/grain filling).

Interestingly, the model performance considerably improved when σ_{veg}^0 ($\sigma_{V\_RH}^o, \sigma_{V\_RV}^o$) was used as an input for the LAI retrieval (i.e. after removing the effect of underlying/background soil cover using WCM). The 2-18-1 topology gave the optimum results while the overall R^2 increased to 0.76 (Table 5). The RMSE of the validation dataset dropped by almost 46.7% in comparison to the previous case while IA for validation dataset surged to 0.92 (Table 5), indicating the superiority of this model in LAI retrieval over the other one. This is evident from the Fig. 12c where the horizontal axis represents the observed LAI values while the vertical axis is the LAI estimated by the NN. Except for a few points, the majority of them fall in the vicinity of 1:1 line while those in Fig. 12a are more scattered.

3.3.2. Plant volume (PV)

The feed-forward neural network trained by LM algorithm with σ_{total}^0 ($\sigma_{T\_RH}^o, \sigma_{T\_RV}^o$) as input retrieved the PV with highest overall R^2 of 0.80 (Table 5). Quite satisfactory results were obtained when this network was applied on the validation dataset, as it estimated the PV values with the RMSE of $1.51\,cm^3/m^2$ while the MAPE was 17.82% (Table 5, Fig. 13a, b). The results dramatically improved by substituting the total backscatter with vegetation backscatter values (Fig. 13c, d). The practical feasibility of the network for PV retrieval is supported by the fact that the model simulated the independent validation dataset with the RMSE of only $0.85\,cm^3/m^2$ and MAPE of 10.31% (Table 5).

3.3.3. Plant water content (PWC)

To study the combined effect of total RH and RV polarized backscatter on PWC, we created a feed-forward network to yield the RMSE below the specified threshold of $0.5\,kg/m^2$ (Table 3). The estimated PWC values were found to be quite close to the observed ones with the

overall R^2 of 0.82 (Table 5). The model satisfactorily inverted the PWC values with the RMSE of $0.38\,kg/m^2$ (Fig. 14a). PWC retrieval was sequentially optimized by incorporating solely the vegetation effect, although it accounted for only 6% of the unexplained variance of the inversion process that was carried out using the total backscatter values. While the R^2 reached up to 0.87, the RMSE of the validation dataset plunged by almost 55% in comparison to the previous model (Table 5). At the same time, the scatter plot for the validated results of PWC values (Fig. 14c) indicates that the estimated values were in close agreement with the observed ones with considerably low MAPE of 10%.

3.3.4. Wet biomass (WB)

For WB retrieval with σ_{total}^0 ($\sigma_{T_{RH}}^o, \sigma_{T_{RV}}^o$) as input, we trained the network until the error requirement of $< 0.50\,kg/m^2$ was satisfied. The model simulated the WB values with the overall R^2 of 0.63 (Table 5). The network, when applied on the independent dataset, gave a higher RMSE of $0.45\,kg/m^2$. Moreover, the IA was extremely low (0.46) showing the inability of the network to learn the underlying functional relationship well (Table 5). This is emphasized by the scatter plot between the observed and estimated WB values (Fig. 15a), whereby the points are completely off the 1:1 line.

Surprisingly, the model performance improved drastically in the latter case. A comparison of the respective R^2 reveals that roughly 17.5% of the unexplained variance of the previous model was accounted for by this inversion approach. The RMSE reduced by ~44% in comparison to the previous model (Table 5). However, the values were slightly underestimated throughout the season even though the scatter of the points was along the 1:1 line (Fig. 15c).

4. Discussion

Our literature review unveiled a vast diversity in the canopy descriptors (in WCM) that are used to model the backscatter from remote sensing data, with no clear agreement on which of them perform best. In addition, there is a lack of prior knowledge about the correlation of crop biophysical parameters with hybrid-polarized backscatter. We, therefore, set up four scenarios, in which we analysed the effect of the
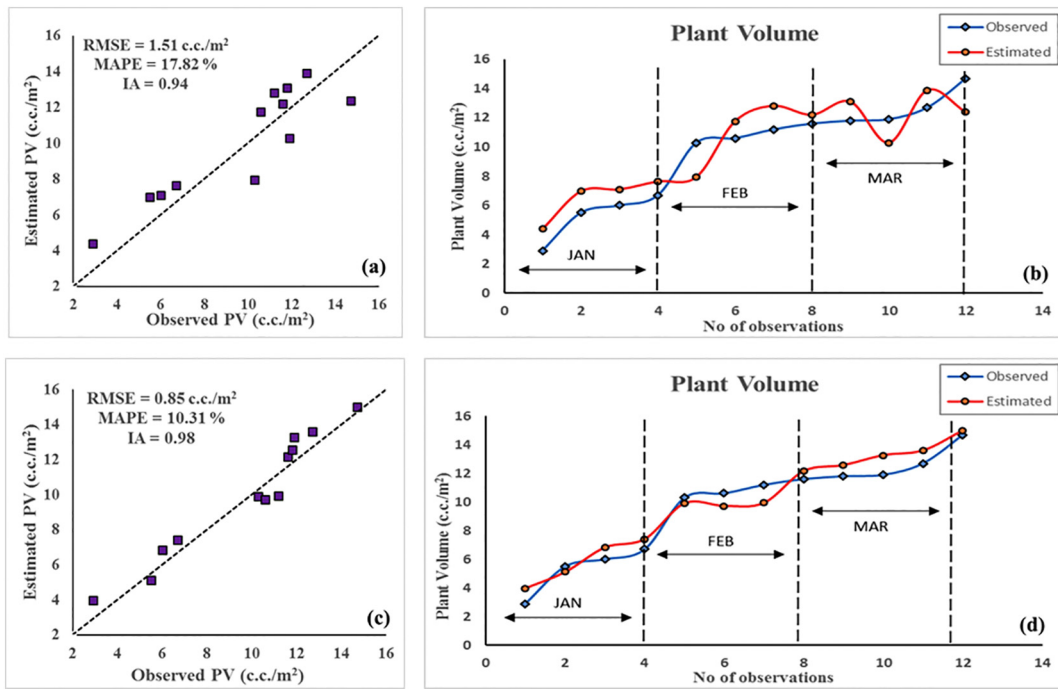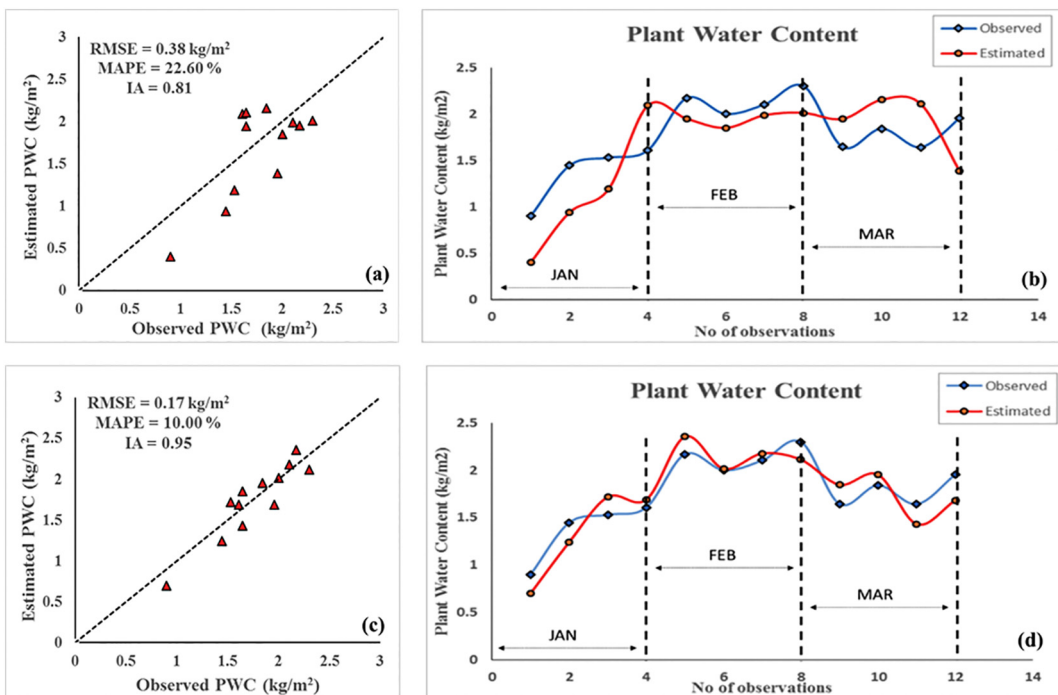
Fig. 13. Scatter plot (a, c) & multi-temporal (b, d) variation of the observed and estimated PV across the season (number of samples N = 12). a, b correspond to the crop parameters retrieved from σ_{total}^{0} ($\sigma_{T\_RH}^{o}, \sigma_{T\_RV}^{o}$) and c, d correspond to those retrieved from σ_{veg}^{0} ($\sigma_{V\_RH}^{o}, \sigma_{V\_RV}^{o}$).

Fig. 14. Scatter plot (a, c) & multi-temporal (b, d) variation of the observed and estimated PWC across the season (number of samples N = 12). a, b correspond to the crop parameters retrieved from σ_{total}^{0} ($\sigma_{T\_RH}^{o}, \sigma_{T\_RV}^{o}$) and c, d correspond to those retrieved from σ_{veg}^{0} ($\sigma_{V\_RH}^{o}, \sigma_{V\_RV}^{o}$).

combination of different canopy descriptors on the accuracy of the total (and henceforth vegetation) backscatter coefficient estimates from RISAT-1 data. This study also demonstrates the feasibility of retrieving wheat biophysical parameters from soil-corrected vegetation backscatter coefficients and the potential to estimate these coefficients using a simple water cloud model-based approach. This capability is examined by comparative evaluation of different canopy descriptors and henceforth, the retrieval accuracy of the crop parameters from total and vegetation backscatter coefficients. Good agreements are obtained

between all the crop parameters and vegetation backscatter coefficients (as shown in Table 5).

4.1. Performance of different canopy descriptors in water cloud model

LAI characterises the density of a canopy cover in relation to its leaf size and thus, plays an active role in attenuating the σ^0 from canopy cover. Ground-based LAI (as the two canopy descriptors) had the least agreement with RISAT-1 derived total backscatter coefficients. A high
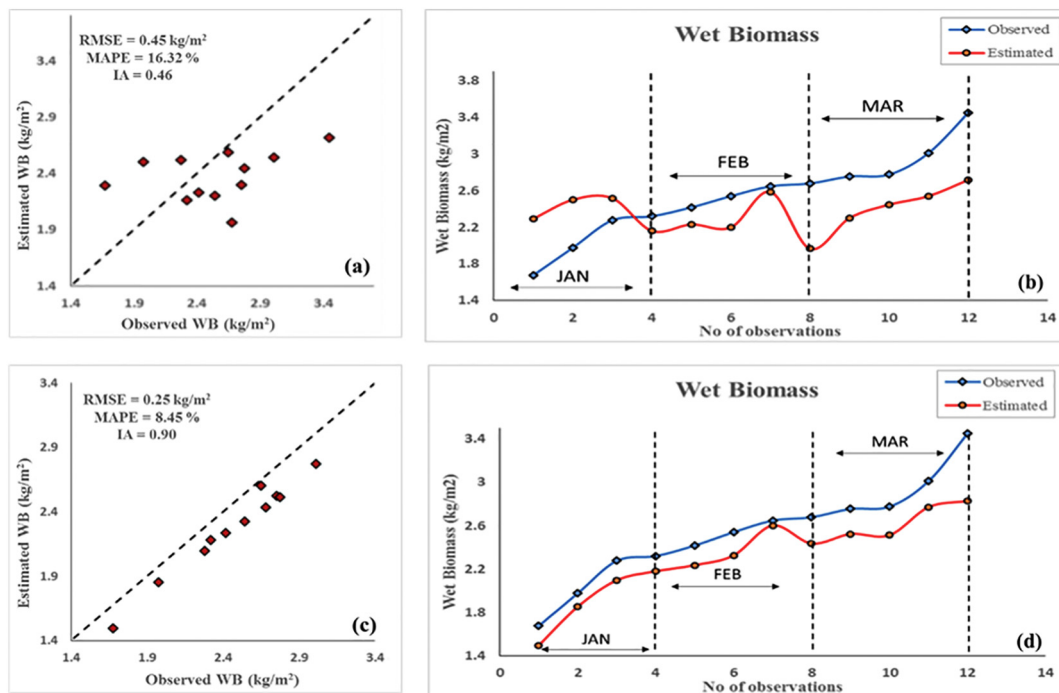
Fig. 15. Scatter plot (a, c) & multi-temporal (b, d) variation of the observed and estimated WB across the season (number of samples $N = 12$). a, b correspond to the crop parameters retrieved from σ_{total}^{0} ($\sigma_{T\_RH}^{o}, \sigma_{T\_RV}^{o}$) and c, d correspond to those retrieved from σ_{veg}^{0} ($\sigma_{V\_RH}^{o}, \sigma_{V\_RV}^{o}$).

degree of overestimation of total backscatter was observed in comparison to the other cases. The primary cause of this discrepancy is likely attributable to the fact that LAI accounts only for the area of vegetation leaves and models the backscatter signal interacting with this area while neglecting the dielectric properties, which also have a substantial impact on the attenuation of backscatter signal. As a result, we observed that the retrieval accuracy of total backscatter values derived using LAI-PWC and LWAI-LWAI as the canopy descriptors was slightly higher than in the previous case. The results were, however, still not encouraging as the model again overestimated the σ_{RH}^{o} and σ_{RV}^{o} with a high RMSE. This discrepancy can be attributed to the heterogeneous nature of the crop canopy. The interaction of the SAR signal with crop canopy is not uniform throughout since the distribution of volume and moisture in each component of the wheat crop (like head, leaf, and stem) varies quite significantly in a heterogeneous manner.

Our results suggest that LAI and IF can accurately model the total backscatter values derived from RISAT-1 data, with very low root mean square error. As discussed earlier, the major setback of the previous models is that neither of them accounts for density and dielectric heterogeneity of the plant cover precisely. The model using LAI and IF as variables largely overcomes the flaws that exist in previous methodologies. In this scenario, LAI like in the other models characterises the density of a vegetation cover with respect to the leaf size but more importantly, IF is responsible for this improved performance. We know that in C-band, the crop canopy functions distinctly as an inhomogeneous medium with all the constituents responding discretely to the incident EM wave thus causing anisotropic absorption and scattering (Maity et al., 2004). Additionally, in case of a wheat plant, the received SAR backscatter is a composite of its interaction with the head, leaves, and stem (Patel et al., 2006a). The distribution of moisture, as well as volume in each of these components, determines the way the signal will interact and penetrate into the crop, and thus, neither of them alone has the capability of fully describing the SAR backscatter.

With IF plant parameter, it is attempted to encompass the most significant crop parameters that can efficiently characterise the backscatter response. The model primarily benefits from the incorporation of crop water and volume information along the crop length (i.e.

height). The distribution of moisture within a confined volume varies heterogeneously, and failure to incorporate this heterogeneity in the previous models increases uncertainty, particularly over high LAI areas.

4.2. Comparative analysis of the retrieval of crop parameters from total and vegetation backscatter coefficients

The inter-comparison of crop parameter values with respect to total and vegetation backscatter coefficient values led to some interesting findings. Crop parameter estimates considerably improved when σ_{veg}^{0} ($\sigma_{V\_RH}^{o}, \sigma_{V\_RV}^{o}$) was used as input in the ANN and had lower RMSE values than σ_{total}^{0} ($\sigma_{T\_RH}^{o}, \sigma_{T\_RV}^{o}$). For instance, in case of LAI, the σ_{veg}^{0} based inversion results (Fig. 12d) were quite consistent with the general LAI trend over the season (increased until heading and then decreased until senescence), especially in the initial and later period of wheat growth. A slight underestimation in the results was seen in the booting/heading stage (LAI > 3) which could have been due to the saturation of the backscatter values beyond this LAI range. The results were still promising in comparison to $\sigma_{total}^{0}\sigma_{total}^{0}$ ($\sigma_{T\_RH}^{o}, \sigma_{T\_RV}^{o}$) based approach. Even for PV and PWC, the elimination of the effect of background soil effectively corrected the simulation trajectory (Figs. 13d and 14d, respectively) especially regarding the shifts and underestimates that were quite evident when the effect was not accounted for (Figs. 13b and 14b, respectively). It is important to highlight here that the SAR backscatter from a vegetated field is uniquely sensitive to the plant volume and its dielectric properties, as has been confirmed by several studies (Kurosu et al., 1995; Patel et al., 2006a), thus explaining the high R^2 values in both the cases.

On the other hand, highest bias was observed in WB values (retrieved from σ_{total}^{0}) throughout the growing season, which resulted in almost a steady trend (estimated values fluctuated between 1.96 and 2.71 kg/m^2 only while the observed range was 1.6 to 3.5 kg/m^2) as shown in Fig. 15b. The disparity was still less in the earlier part of the season while few discrepancies up to 0.7 kg/m^2 were observed as the biomass values increased. Like LAI, it can be interpreted as part of the saturation effect, in which the resultant backscatter becomes insensitive to the variability in biomass as the plant grows. The similar

disagreement has been discussed in several papers (Del Frate et al., 2004; Jia et al., 2013; Satalino et al., 2015). The shift was significantly reduced, once the input was substituted with σ_{veg}^0 (Fig. 15d). This is in line with earlier findings that report that at steep incidence angles (like in this study), the relationship between σ^o and wet biomass is substantially affected by the soil characteristics, specifically by the soil moisture content (Luciani et al., 1994).

We know that the vegetation canopy, which is itself a volume of scattering constituents, is bounded by a scattering soil surface. Particularly in C-band, the total backscatter that we obtain from SAR data includes the contribution from both vegetation and background soil cover. Furthermore, the studies have confirmed that the attenuation in radar signal from soil increases with the incidence angle (Brown et al., 2003). We conjecture that the mixed response from soil and crop canopy hampers the retrieval of crop biophysical parameters and therefore should be resolved. This is especially true in early growth stages (LAI < 2) when the canopy cover is less dense with more soil exposed and is evident in the results obtained. Our results suggest that the retrieval of LAI, PV, PWC and WB can be significantly improved once we eliminate the effect of background soil. They also testify the relevance of applying a simple WCM based modelling approach, even if the crop canopy is expressed as two layers (i.e. vegetation and soil) with only two descriptors (LAI and IF) representing the complexity of the vegetation cover. Few discrepancies that exist could be due to the negation of soil-stem scattering component whose effect is more pronounced at later stages since there is an overall increase in crop volume.

5. Conclusions

The study aimed to explore the potential of hybrid-polarized RISAT-1 SAR data for the retrieval of wheat crop biophysical parameters (LAI, PV, PWC and WB) on a regional scale by using soil-corrected hybrid-polarized vegetation backscatter or σ_{veg}^0 ($\sigma_{V\_RH}^o$, $\sigma_{V\_RV}^o$). The total backscatter or σ_{total}^0 ($\sigma_{T\_RH}^o$, $\sigma_{T\_RV}^o$) received from a vegetated field is a composite of the contribution from the vegetation as well as the underlying soil surface. We hypothesized that refining the σ_{total}^0 into a soil corrected σ_{veg}^0 would result in more accurate estimation of crop parameters. The rationale being that the underlying/background soil acts as noise in such crop parameter retrieval applications and thus its effect must be eliminated.

A semi-empirical water cloud model was used to refine σ_{total}^0. Several model parameterisation schemes (in the form of canopy descriptors) were evaluated to account for the vertical heterogeneity of the crop canopy. A comprehensive analysis of the measured and estimated RH and RV backscatter revealed the very high sensitivity of the combined effect of LAI (as V_1) and interaction factor (as V_2) on the σ_{total}^0. Our analytical results also revealed a clear and consistent relationship between hybrid-polarized backscatter and wheat crop biophysical parameters over the growing season. The MLP neural networks were applied to the dataset to evaluate and compare the effectiveness of the two methods (σ_{total}^0 and σ_{veg}^0 as inputs) in the estimation of crop parameters. The results revealed a high correlation of PV ($R^2 = 0.80$) and PWC ($R^2 = 0.82$) with σ_{total}^0. However, the relationship improved substantially when σ_{total}^0 was substituted with σ_{veg}^0 (R^2 increased to 0.89 and 0.87, for PV and PWC respectively), especially in the initial stages of the growing season, when the maximum soil is exposed. This responsiveness is attributable to the unique sensitivity of SAR backscatter to dielectric properties of the crop volume and elimination of the contribution from underlying soil. In the estimation of LAI and WB, the predictive ability was relatively poorer with σ_{total}^0 but improved significantly with σ_{veg}^0. The σ_{total}^0 saturated at LAI of approximately 3 m^2/m^2 and WB of 2.7 kg/m^2. In conclusion, the effect of underlying soil in narrow leaf crops such as wheat is significant and hence should not be disregarded.

The novelty of this study stems from the fact that it is a first step towards the retrieval of crop biophysical parameters using RISAT-1 SAR

hybrid-polarized data. The analytical findings have a potential to serve as a reference for further research initiatives that would attempt to relate the crop biophysical parameters to hybrid-polarized backscatter coefficients. Modelling the backscatter using LAI and IF as the canopy descriptors in WCM and substituting σ_{total}^0 with σ_{veg}^0, can considerably improve the accuracy of retrieving crop biophysical parameters with hybrid-polarized datasets. Future research can be directed towards the synergistic use of multi-polarimetric, multi-frequency or multi-sensor data, in addition to the time series dataset used in this study. As the insights about crop dynamics, their underlying processes and interactions are improving, greater research prospects seem to be emerging in the field of crop growth modelling and assimilating the remote sensing data into models such as CERES-wheat. This will allow for a profound understanding of different processes that govern crop growth.

References

Attema, E.P.W., Ulaby, F.T., 1978. Vegetation modeled as a water cloud. Radio Sci. 13 (2), 357–364. http://dx.doi.org/10.1029/rs013i002p00357.

Battude, M., Al Bitar, A., Morin, D., Cros, J., Huc, M., Sicre, C.M., Demarez, V., 2016. Estimating maize biomass and yield over large areas using high spatial and temporal resolution Sentinel-2 like remote sensing data. Remote Sens. Environ. 184, 668–681. http://dx.doi.org/10.1016/j.rse.2016.07.030.

Bouman, B.A.M., 1991. Crop parameter estimation from ground-based X-band (3-cm wave) radar backscattering data. Remote Sens. Environ. 37 (3), 193–205. http://dx.doi.org/10.1016/0034-4257(91)90081-g.

Bouman, B.A., van Kasteren, H.W., 1990. Ground-based X-band (3-cm wave) radar backscattering of agricultural crops. II. Wheat, barley, and oats; the impact of canopy structure. Remote Sens. Environ. 34 (2), 107–119. http://dx.doi.org/10.1016/0034-4257(90)90102-r.

Brown, S., Quegan, S., Morrison, K., Bennett, J.C., Cookmartin, G., 2003. High-resolution measurements of scattering in wheat canopies-implications for crop parameter retrieval. IEEE Trans. Geosci. Remote Sens. 41 (7), 1602–1610. http://dx.doi.org/10.1109/tgrs.2003.814132.

Ceccato, P., Flasse, S., Tarantola, S., Jacquemoud, S., Grégoire, J.M., 2001. Detecting vegetation leaf water content using reflectance in the optical domain. Remote Sens. Environ. 77 (1), 22–33. http://dx.doi.org/10.1016/s0034-4257(01)00191-2.

Charbonneau, F.J., Brisco, B., Raney, R.K., McNairn, H., Liu, C., Vachon, P.W., Shang, R., DeAbreu, C., Merzouki, A., Geldsetzer, T., 2010. Compact polarimetry overview and applications assessment. Can. J. Remote Sens. 36 (sup2), S298–S315. http://dx.doi.org/10.5589/m10-062.

Colombo, R., Bellingeri, D., Fasolini, D., Marino, C.M., 2003. Retrieval of leaf area index in different vegetation types using high resolution satellite data. Remote Sens. Environ. 86 (1), 120–131. http://dx.doi.org/10.1016/s0034-4257(03)00094-4.

Cookmartin, G., Saich, P., Quegan, S., Cordey, R., Burgess-Allen, P., Sowter, A., 2000. Modeling microwave interactions with crops and comparison with ERS-2 SAR observations. IEEE Trans. Geosci. Remote Sens. 38 (2), 658–670. http://dx.doi.org/10.1109/36.841996.

Dabrowska-Zielinska, K., Inoue, Y., Kowalik, W., Gruszczynska, M., 2007. Inferring the effect of plant and soil variables on C- and L-band SAR backscatter over agricultural fields, based on model analysis. Adv. Space Res. 39 (1), 139–148. http://dx.doi.org/10.1016/j.asr.2006.02.032.

Del Frate, F., Wang, L.F., 2001. Sunflower biomass estimation using a scattering model and a neural network algorithm. Int. J. Remote Sens. 22 (7), 1235–1244. http://dx.doi.org/10.1080/01431160151144323.

Del Frate, F., Ferrazzoli, P., Guerriero, L., Strozzi, T., Wegmüller, U., Cookmartin, G., Quegan, S., 2004. Wheat cycle monitoring using radar data and a neural network trained by a model. IEEE Trans. Geosci. Remote Sens. 42 (1), 35–44. http://dx.doi.org/10.1109/tgrs.2003.817200.

Doraiswamy, P.C., Sinclair, T.R., Hollinger, S., Akhmedov, B., Stern, A., Prueger, J., 2005. Application of MODIS derived parameters for regional crop yield assessment. Remote Sens. Environ. 97 (2), 192–202. http://dx.doi.org/10.1016/j.rse.2005.03.015.

El Hajj, M., Baghdadi, N., Zribi, M., Belaud, G., Cheviron, B., Courault, D., Charron, F., 2016. Soil moisture retrieval over irrigated grassland using X-band SAR data. Remote Sens. Environ. 176, 202–218. http://dx.doi.org/10.1016/j.rse.2016.01.027.

Ferrazzoli, P., Guerriero, L., Paloscia, S., Pampaloni, P., Solimini, D., 1992. Modeling polarization properties of emission from soil covered with vegetation. IEEE Trans. Geosci. Remote Sens. 30 (1), 157–165. http://dx.doi.org/10.1109/36.124226.

Ferrazzoli, P., Paloscia, S., Pampaloni, P., Schiavon, G., Sigismondi, S., Solimini, D., 1997. The potential of multifrequency polarimetric SAR in assessing agricultural and arboreous biomass. IEEE Trans. Geosci. Remote Sens. 35 (1), 5–17. http://dx.doi.org/

10.1109/36.551929.

Green Jr., P.E., 1968. Radar measurements of target scattering properties. In: Evans, J.V., Hagfors, T. (Eds.), Radar Astronomy. McGraw-Hill Book Company, New York, pp. 1–78.

Hégarat-Mascle, L., Zribi, M., Alem, F., Weisse, A., Loumagne, C., 2002. Soil moisture estimation from ERS/SAR data: toward an operational methodology. IEEE Trans. Geosci. Remote Sens. 40 (12), 2647–2658. http://dx.doi.org/10.1109/tgrs.2002.806994.

Jia, M., Tong, L., Chen, Y., Wang, Y., Zhang, Y., 2013. Rice biomass retrieval from multitemporal ground-based scatterometer data and RADARSAT-2 images using neural networks. J. Appl. Remote Sens. 7 (1), 073509. http://dx.doi.org/10.1117/1.jrs.7.073509.

Kogan, F., Kussul, N., Adamenko, T., Skakun, S., Kravchenko, O., Kryvobok, O., Shelestov, A., Kolotii, A., Kussul, O., Lavrenyuk, A., 2013. Winter wheat yield forecasting in Ukraine based on Earth observation, meteorologicaldata and biophysical models. International Journal of Applied Earth Observation and Geoinformation 23 (1), 192–203. http://dx.doi.org/10.1016/j.jag.2013.01.002.

Kumar, P., Prasad, R., Mishra, V.N., Gupta, D.K., Singh, S.K., 2016. Artificial neural network for crop classification using C-band RISAT-1 satellite datasets. Russ. Agric. Sci. 42 (3–4), 281–284. http://dx.doi.org/10.3103/s1068367416030137.

Kurosu, T., Fujita, M., Chiba, K., 1995. Monitoring of rice crop growth from space using the ERS-1 C-band SAR. IEEE Transactions on Geoscience and Remote Sensing 33 (4), 1092–1096. http://dx.doi.org/10.1109/36.406698.

Lourakis, M.I., 2005. A brief description of the Levenberg-Marquardt algorithm implemented by levmar. Foundation of Research and Technology 4 (1).

Luciani, S., Paloscia, S., Pampaloni, P., Schiavon, G., Sigismondi, S., Solimini, D., 1994. Sensitivity of microwave backscattering to crop biomass. In: Geoscience and Remote Sensing Symposium, 1994. IGARSS'94. Surface and Atmospheric Remote Sensing: Technologies, Data Analysis and Interpretation. vol. 3. pp. 1844–1846. http://dx.doi.org/10.1109/igarss.1994.399584.

Macelloni, G., Paloscia, S., Pampaloni, P., Marliani, F., Gai, M., 2001. The relationship between the backscattering coefficient and the biomass of narrow and broad leaf crops. IEEE Trans. Geosci. Remote Sens. 39 (4), 873–884. http://dx.doi.org/10.1109/36.917914.

Maity, S., Patnaik, C., Chakraborty, M., Panigrahy, S., 2004. Analysis of temporal backscattering of cotton crops using a semiempirical model. IEEE Trans. Geosci. Remote Sens. 42 (3), 577–587.

Marquardt, D.W., 1963. An algorithm for least-squares estimation of nonlinear parameters. J. Soc. Ind. Appl. Math. 11 (2), 431–441. http://dx.doi.org/10.1137/0111030.

Mattia, F., Le Toan, T., Picard, G., Posa, F., DÀlessio, A., Notarnicola, C., Gatti, A., Rinaldi, M., Satalino, G., Pasquariello, G., 2003. Multitemporal c-band radar measurements on wheat fields. IEEE Trans. Geosci. Remote Sens. 41 (7), 1551–1558. http://dx.doi.org/10.1109/tgrs.2003.813531.

McNairn, H., Kross, A., Lapen, D., Caves, R., Shang, J., 2014. Early season monitoring of corn and soybeans with TerraSAR-X and RADARSAT-2. Int. J. Appl. Earth Obs. Geoinf. 28, 252–259. http://dx.doi.org/10.1016/j.jag.2013.12.015.

Mishra, M.D., Patel, P., Srivastava, H.S., Patel, P.R., Shukla, A., Shukla, A.K., 2014. Absolute radiometric calibration of FRS-1 and MRS mode of RISAT-1 synthetic aperture radar (SAR) data using Corner reflectors. Int. J. Adv. Eng. Res. Sci. 1 (6), 78–89.

Misra, T., Rana, S.S., Shankara, K.N., 2005. Synthetic Aperture Radar Payload of Radar Imaging Satellite (RISAT) of ISRO. URSI-GA, Session F-08, Vigyan Bhavan, New Delhi.

Moran, M.S., Vidal, A., Troufleau, D., Inoue, Y., Michell, T.A., 1998. Ku and C-band SAR for discriminating agricultural crop and soil conditions. IEEE Trans. Geosci. Remote Sens. 36 (1), 265–272. http://dx.doi.org/10.1109/36.655335.

Moulin, S., Bondeau, A., Delecolle, R., 1998. Combining agricultural crop models and satellite observations: from field to regional scales. Int. J. Remote Sens. 19 (6), 1021–1036. http://dx.doi.org/10.1080/014311698215586.

Pal, M., Maity, R., Suman, M., Das, S.K., Patel, P., Srivastava, H.S., 2017. Satellite-based probabilistic assessment of soil moisture using C-band quad-polarized RISAT1 data. IEEE Trans. Geosci. Remote Sens. 55 (3), 1351–1362. http://dx.doi.org/10.1109/TGRS.2016.2623378.

Patel, P., Srivastava, H.S., 2007. Polarimetric SAR classification using physical based scattering mechanism: comparative evaluation of L and P bands. In: Conference Proceedings of Joint Experiment Project Towards Microwave Remote Sensing Data Utilisation, Ahmedabad, Ahmedabad, India, pp. 15–20.

Patel, P., Srivastava, H.S., 2013a. Ground truth planning for synthetic aperture radar (SAR): addressing various challenges using statistical approach. Int. J. Adv. Remote Sens. GIS Geogr. 1 (2), 1–17.

Patel, P., Srivastava, H.S., 2013b. RADARSAT-2 announcement of opportunity project on soil moisture, surface roughness and vegetation parameter retrieval using SAR polarimetry. In: SAC/EPSA/MPSG/CVD/TDP R&D/01/13, SOAR International Closing and Reporting–2013.

Patel, P., Srivastava, H.S., Navalgund, R.R., 2006a. Estimating wheat yield: an approach for estimatingnumber of grains using cross-polarised ENVISAT-1 ASAR data. In: Valinia, Azita, Uratsuka, Seiho, Misra, Tapan (Eds.), Microwave Remote Sensing of the Atmosphere and Environment V, Proc. of SPIE, vol. 6410. pp. 641009-1–641009-12. http://dx.doi.org/10.1117/12.693930.

Patel, P., Srivastava, H.S., Panigrahy, S., Parihar, J.S., 2006b. Comparative evaluation of the sensitivity of multi-polarized multi-frequency SAR backscatter to plant density. Int. J. Remote Sens. 27 (2), 293–305. http://dx.doi.org/10.1080/01431160500214050.

Prevot, L., Champion, I., Guyot, G., 1993. Estimating surface soil moisture and leaf area index of a wheat canopy using a dual-frequency (C and X bands) scatterometer.

Remote Sens. Environ. 46 (3), 331–339. http://dx.doi.org/10.1016/0034-4257(93)90053-z.

Quesney, A., Le Hégarat-Mascle, S., Taconet, O., Vidal-Madjar, D., Wigneron, J.P., Loumagne, C., Normand, M., 2000. Estimation of watershed soil moisture index from ERS/SAR data. Remote Sens. Environ. 72 (3), 290–303. http://dx.doi.org/10.1016/s0034-4257(99)00102-9.

Raney, R.K., 2007. Hybrid-polarity SAR architecture. IEEE Trans. Geosci. Remote Sens. 45 (11), 3397–3404. http://dx.doi.org/10.1109/tgrs.2007.895883.

Raney, R.K., 2011. A perspective on compact polarimetry. IEEE Geosci. Remote Sens. Newslett. 160 (160), 12–18.

Saich, P., Borgeaud, M., 2000. Interpreting ERS SAR signatures of agricultural crops in Flevoland, 1993–1996. IEEE Trans. Geosci. Remote Sens. 38 (2), 651–657. http://dx.doi.org/10.1109/36.841995.

Said, S., Kothyari, U.C., Arora, M.K., 2012. Vegetation effects on soil moisture estimation from ERS-2 SAR images. Hydrol. Sci. J. 57 (3), 517–534. http://dx.doi.org/10.1080/02626667.2012.665608.

Satalino, G., Balenzano, A., Mattia, F., Rinaldi, M., Maddaluno, C., Annicchiarico, G., 2015. Retrievalof wheat biomass from multitemporal dual polarised SAR observations. In: 2015 IEEE International Geoscience and RemoteSensing Symposium (IGARSS), pp. 5194–5197. http://dx.doi.org/10.1109/igarss.2015.7327004.

Sivasankar, T., Srivastava, H.S., Sharma, P.K., Kumar, D., Patel, P., 2015. Study of hybrid polarimetric parameters generated from Risat-1 SAR data for various land cover targets. Int. J. Adv. Remote Sens. GIS Geogr. 3, 32–42.

Souyris, J.C., Imbo, P., Fjortoft, R., Mingot, S., Lee, J.S., 2005. Compact polarimetry based on symmetry properties of geophysical media: the π/4 mode. IEEE Trans. Geosci. Remote Sens. 43 (3), 634–646. http://dx.doi.org/10.1109/tgrs.2004.842486.

Srivastava, H.S., Patel, P., Manchanda, M.L., Adiga, S., 2002. An attempt to incorporate the effect of crop cover in soil moisture estimation using multi-incidence angle Radarsat-1 SAR data. Asian J. Geoinformatics 2 (3), 33–40.

Srivastava, H.S., Patel, P., Manchanda, M.L., Adiga, S., 2003. Use of multi-incidence angle RADARSAT-1 SAR data to incorporate the effect of surface roughness in soil moisture estimation. IEEE Trans. Geosci. Remote Sens. 41 (7), 1638–1640. http://dx.doi.org/10.1109/tgrs.2003.813356.

Srivastava, H.S., Patel, P., Navalgund, R.R., 2006a. Application potentials of synthetic aperture radar interferometry for land-cover mapping and crop-height estimation. Curr. Sci. 91 (6), 783–788.

Srivastava, H.S., Patel, P., Navalgund, R.R., 2006b. Incorporating soil texture in soil moisture estimation from extended low-1 beam mode RADARSAT-1 SAR data. Int. J. Remote Sens. 27 (12), 2587–2598. http://dx.doi.org/10.1080/01431160500497838.

Srivastava, H.S., Patel, P., Prasad, S.N., Sharma, Y., Khan, B.A., Praveen, B., Prasad, K.C.A., Sharma, S., Vijayan, L., Vijayan, V.S., 2008. Potential applications of multi-parameteric synthetic aperture radar (SAR) data in wetland inventory: a case study of Keoladeo National Park (A World Heritage and Ramsar site), Bharatpur, India. In: Proc. 12th World Lake Conference, TAAL, pp. 1862–1879.

Srivastava, H.S., Patel, P., Sharma, Y., Navalgund, R.R., 2009. Large-area soil moisture estimation using multi-incidence-angle RADARSAT-1 SAR data. IEEE Trans. Geosci. Remote Sens. 47 (8), 2528–2535. http://dx.doi.org/10.1109/tgrs.2009.2018448.

Srivastava, H.S., Patel, P., Sharma, K.P., Krishnamurthy, Y.V.N., Dadhwal, V.K., 2011. A semi-empirical modelling approach to calculate two-way attenuation in radar backscatter from soil due to crop cover. Curr. Sci. 100 (12), 1871–1874.

Taconet, O., Benallegue, M., Vidal-Madjar, D., Prevot, L., Dechambre, M., Normand, M., 1994. Estimation of soil and crop parameters for wheat from airborne radar back-scattering data in C and X bands. Remote Sens. Environ. 50 (3), 287–294. http://dx.doi.org/10.1016/0034-4257(94)90078-7.

Toure, A., Thomson, K.P., Edwards, G., Brown, R.J., Brisco, B.G., 1994. Adaptation of the MIMICS backscattering model to the agricultural context-wheat and canola at L and C bands. IEEE Trans. Geosci. Remote Sens. 32 (1), 47–61. http://dx.doi.org/10.1109/36.285188.

Tsang, L., Ding, K.H., Zhang, G., Hsu, C.C., Kong, J.A., 1995. Backscattering enhancement and clustering effects of randomly distributed dielectric cylinders overlying a dielectric half space based on Monte-Carlo simulations. IEEE Trans. Antennas Propag. 43 (5), 488–499. http://dx.doi.org/10.1109/8.384193.

Ulaby, F.T., Bush, T.F., 1976. Monitoring wheat growth with radar. Photogramm. Eng. Remote. Sens. 42 (4), 557–568.

Ulaby, F.T., Wilson, E.A., 1985. Microwave attenuation properties of vegetation canopies. IEEE Trans. Geosci. Remote Sens. GE-23 (5), 746–753. http://dx.doi.org/10.1109/tgrs.1985.289393.

Ulaby, F.T., Moore, R.K., Fung, A.K., 1986. Microwave Remote Sensing Active and Passive-Volume III: From Theory to Applications.

Ulaby, F.T., Sarabandi, K., Mcdonald, K.Y.L.E., Whitt, M., Dobson, M.C., 1990. Michigan microwave canopy scattering model. Int. J. Remote Sens. 11 (7), 1223–1253. http://dx.doi.org/10.1080/01431169008955090.

Uppala, D., Venkata, R.K., Poloju, S., Venkata Rama, S.M., Dadhwal, V.K., 2016. Discrimination of maize crop with hybrid polarimetric RISAT1 data. Int. J. Remote Sens. 37 (11), 2641–2652. http://dx.doi.org/10.1080/01431161.2016.1184353.

Wang, Y., Dong, D., 1997. Retrieving forest stand parameters from SAR backscatter data using a neural network trained by a canopy backscatter model. Int. J. Remote Sens. 18 (4), 981–989. http://dx.doi.org/10.1080/014311697218872.

Wang, C., Wu, J., Zhang, Y., Pan, G., Qi, J., Salas, A.W., 2009. Characterizing L-band scattering of paddy rice in Southeast China with radiative transfer model and multitemporal ALOS/PALSAR imagery. IEEE Trans. Geosci. Remote Sens. 47 (4), 988–998. http://dx.doi.org/10.1109/tgrs.2008.2008309.

Zribi, M., Dechambre, M., 2003. A new empirical model to retrieve soil moisture and roughness from C-band radar data. Remote Sens. Environ. 84 (1), 42–52. http://dx.doi.org/10.1016/s0034-4257(02)00069-x.